(A New Proposal to Jefferson Lab PAC-30)

Probing Quark-Gluon Correlations in the Neutron: A Precision Measurement of the Neutron g_2 and d_2 at High Q^2 in Hall A

S. Zhou and X. Li
China Institute of Atomic Energy, Beijing 102413, P.R. China

P. Markowitz
Florida International University, Miami, FL 33199, USA

A. Camsonne, J.-P. Chen (co-spokesperson), E. Chudakov, J.-O. Hansen, D.W. Higinbotham, M. Jones, A. Saha, B. Wojtsekhowski
Jefferson Lab, Newport News, VA 23606, USA

G.G. Petratos
Kent State University, Kent, OH 44242, USA

W. Korsch (co-spokesperson)
University of Kentucky, Lexington, KY 40506, USA

K. Kumar, K. Paschke[1]
University of Massachusetts Amherst, Amherst, MA 01003, USA

W. Bertozzi, S. Gilad, X. Zheng[1]
Massachusetts Institute of Technology, Cambridge, MA 02139, USA

F.R. Wesselmann
Norfolk State University, Norfolk, VA 23504, USA

A. Ahmidouch, S. Danagoulian
North Carolina A&T State University, Greensboro, NC 27411, USA

R. Gilman
Rutgers University, Piscataway, NJ 08855, USA

H. Lu, X. Yan and Y. Ye
University of Science and Technology of China, Hefei, Anhui 230026, P.R. China

Seonho Choi, Hyekoo Kang, Byungwuek Lee, Yumin Oh, Jongsog Song
Seoul National University, Seoul 151-747, South Korea

P. Souder
Syracuse University, Syracuse, NY 13244

A. Lukhanin, Z.-E. Meziani, B. Sawatzky (co-spokesperson)
Temple University, Philadelphia, PA 19122, USA

G. Cates, N. Liyanage, B. Norum, K. Slifer
University of Virginia, Charlottesville, VA 22901, USA

D. Armstrong, T. Averett (co-spokesperson), J. M. Finn, K. Griffioen, A. Kelleher, V. Sulkosky
College of William and Mary, Williamsburg, VA 23185, USA

July 10, 2006

Contact: Brad Sawatzky (brads@jlab.org)

[1] Affiliation starting September 2006: University of Virginia, Charlottesville, VA 22904

Abstract

We propose to measure the unpolarized cross section $\sigma_0^{^3He}$, the parallel asymmetry $A_\parallel^{^3He}$ and the perpendicular asymmetry $A_\perp^{^3He}$ to extract the g_2 structure function in the large x region with good precision. We will use the longitudinally polarized (P_b = 0.80) CEBAF electron beam and a 40 cm-long high pressure polarized ^{3}He target. The measurement will be performed using two kinematic configurations:

- E_{beam} = 8.8 GeV, with the spectrometers at $\theta = \pm 30.0^\circ$
- E_{beam} = 6.6 GeV, with the spectrometers at $\theta = \pm 40.0^\circ$

The kinematic region involved in this proposal involves $0.2 < x < 0.95$ and $2.5 < Q^2 < 10 \mathrm{GeV}^2/c^2$

At each beam energy the BigBite spectrometer will be used to acquire the asymmetry data (perpendicular and parallel) while the left arm HRS spectrometer will be used to measure the absolute cross section. Both spectrometers will be set to equal scattering angles on each side of the incident beam line. BigBite's mode of operation is such that a single magnetic field setting will cover the entire kinematic range at each beam energy. The left HRS central momentum will be stepped across the same kinematic range to measure the absolute cross section as a function of x. The target polarization orientation will be set transverse or longitudinal to the beam with a value of P_t = 0.50 while the beam helicity will be reversed at a rate of 30 Hz. A beam current of 10 μA combined with a 30 cm long target (after cuts) of density 12 amg provides a luminosity of 5×10^{35} cm^{-2}s^{-1}. We request 200 hours for the 6.6 GeV kinematics and 400 hours for the 8.8 GeV setting. With the inclusion of an additional 100 hours for overhead and calibration, the total beam request is 700 hours, or roughly 29 days of beam.

The focus of the proposed measurement is two-fold:

1. precisely measuring the Q^2 dependence of the neutron g_2 for $0.5 < x < 0.9$, something that has never been done high-x, high-Q^2 region; and
2. combine the proposed data with those of the lower energy d_2^n measurement E04-016, to significantly improve knowledge of the Q^2 dependence of the d_2^n matrix element at Q^2 = 3.0 and 4.0 GeV$^2/c^2$.

The quantity $d_2^n = \int_0^1 \bar{g}_2 \, dx = \int_0^1 x^2(2g_1 + 3g_2) \, dx$ is related to the twist three matrix element in the Operator Product Expansion (OPE) framework. It is a direct measure of the quark-gluon correlations within the nucleon and reflects the response of the *color* electric and magnetic fields to the polarization of the nucleon (alignment of its spin along one direction). This quantity has seen considerable study in Lattice QCD and is one of the cleanest observables with which to test the theory.

We would also like to comment on a "sister" experiment in Hall C that has also been submitted to the PAC30 board. The kinematic coverage of the Hall A measurement has been specifically selected to compliment the coverage of the Hall C proposal. BigBite in Hall A is ideally suited to map out the the high-x, high-Q^2 region is reasonable time and without tying up the highest energy Hall. In contrast, the SHMS/HMS in Hall C is uniquely suited to make a definitive measurement of the Q^2 evolution of d_2^n due to its remarkably flat Q^2 coverage per bin over $0.4 < x < 1$. BigBite is not able to match this feat due to rate limitations were it moved sufficiently far forward. Together, the two measurements would provide a truly exceptional understanding of the structure function $g_2^n(x, Q^2)$, $d_2^n(Q^2)$, and the associated quark-gluon correlations within the nucleon.

Contents

1 Technical participation of research groups

After thorough discussion with Hall A and JLab administration, Temple University, the College of William and Mary, and the University of Kentucky will jointly commit to providing two full-time equivalent (FTE) manpower to the upgrade of Hall A. The Chinese collaboration (USTC and CIAE) intend to commit an additional 1–2 FTE manpower. This effort will be devoted to successfully commissioning the following base equipment items:

- the upgraded HRS DAQ systems,
- Moeller polarimeter, and
- the Compton polarimeter.

These personnel would be assigned to work in conjunction with the dedicated Hall A staff. Funding for these FTE's will come from existing DOE grants and the institutions involved and will *not* constitute an additional DOE funding request.

In addition, the Chinese collaboration (USTC and CIAE) intent to commit 1–2 FTE to help commissioning

Beyond the baseline equipment, the polarized ^{3}He group will facilitate the development and installation of the polarized 3He target for Hall A. This target has seen tremendous demand in Hall A in recent years and will no doubt be an equally critical component for Hall A's 12 GeV program.

2 Introduction and Motivation

In inclusive polarized lepton-nucleon deep-inelastic scattering, one can access two spin-dependent structure functions of the nucleon, g_1 and g_2. In the last twenty five years, measurements of g_1 have been used to test Quantum Chromodynamics (QCD) through the Björken sum rule and investigate the spin content of the nucleon in term of its constituents. While g_1 can be understood in terms of the Feynman parton model which describes the scattering in terms of *incoherent* parton scattering, g_2 cannot. Rather, one has to consider parton correlations initially present in the target nucleon, and the associated process is given a *coherent* parton scattering in the sense that more than one parton takes part in the interaction. Indeed, using the operator product expansion (OPE) [6, 7], it is possible to interpret the g_2 spin structure function beyond the simple quark-parton model as a higher twist structure function. As such, it is exceedingly interesting because it provides a unique opportunity to study the quark-gluon correlations in the nucleon which cannot otherwise be accessed.

In a recent review Filippone and Ji [8] explained that most higher-twist processes cannot be cleanly separated from the leading twist because of the so-called infrared renormalon problem first recognized by t'Hooft. This ambiguity arises from separating quarks and gluons pre-existing in the hadron wave function from those produced in radiative processes. Such a separation turns out to be always scheme dependent. However, the g_2 structure function is an *exception* because it contributes at the leading order to the spin asymmetry of longitudinally-polarized lepton scattering on transversely-polarized nucleons. Thus, g_2 **is among the cleanest higher-twist observables**.

Why does the g_2 structure function contain information about the quark and gluon correlations in the nucleon? From the optical theorem, g_2 is the imaginary part of the spin-dependent Compton amplitude for the process $\gamma^*(+1)+N(+1/2) \rightarrow \gamma^*(0)+N(-1/2)$,

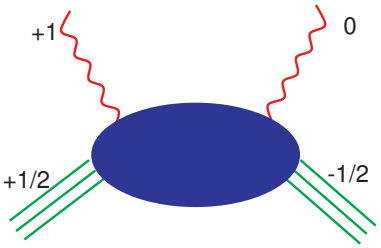

Figure 1: Compton amplitude of $\gamma^*(+1)+N(+1/2) \rightarrow \gamma^*(0)+N(-1/2)$.

where γ^* and N denote the virtual photon and the nucleon, respectively, and the numbers in the brackets are the helicities. Thus this Compton scattering involves the t-channel helicity exchange $+1$. When factorized in terms of parton sub-processes, the intermediate partons must carry this helicity exchange. Because chirality is conserved in vector coupling, massless quarks in perturbative processes cannot produce a helicity flip. QCD allows this helicity exchange to occur in two ways (see Fig. 2): first, single quark scattering in which the quark carries one unit of orbital angular momentum through its transverse momentum wave function; second, quark scattering with an additional transversely-polarized gluon from the nucleon target. The two mechanisms are combined in such a way to yield a gauge-invariant result. Consequently, g_2 provides a direct probe of the quark-gluon correlations in the nucleon wave function.

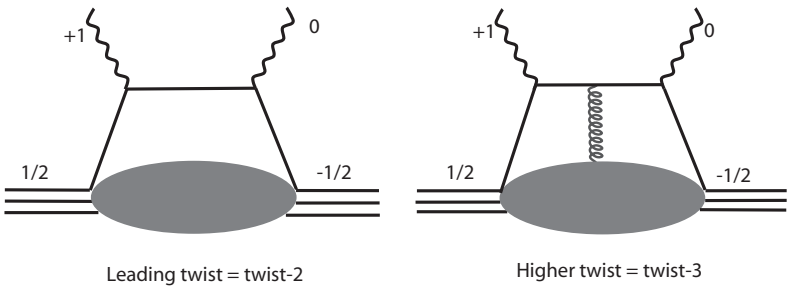

Figure 2: Twist-two and twist-three contributions to virtual Compton scattering

2.1 The twist-three reduced matrix element

The piece of interesting physics we want to focus on in this proposal is contained in the second moment in x of a linear combination of g_1 and g_2, namely

$$\begin{aligned} d_2(Q^2) &= \int_0^1 x^2 \left[2g_1(x,Q^2) + 3g_2(x,Q^2)\right] dx \quad (1) \\ &= 3\int_0^1 x^2 \left[g_2(x,Q^2) - g_2^{WW}(x,Q^2)\right] dx \quad (2) \\ &= 3\int_0^1 x^2 \left[\bar{g_2}(x,Q^2)\right] dx \end{aligned}$$

where g_2^{WW}, known as the Wandzura-Wilczek [9] term, depends only on g_1

$$g_2^{WW}(x,Q^2) = -g_1(x,Q^2) + \int_x^1 \frac{g_1(y,Q^2)}{y} dy. \quad (3)$$

and

$$\bar{g_2}(x,Q^2) = -\int_x^1 \frac{dy}{y}\frac{d}{dy}\left[\frac{m}{M}h_T(y,Q^2) + \xi(y,Q^2)\right] \quad (4)$$

is expressed in terms of the transverse polarization density $h_T(x,Q^2)$ function (Transversity) suppressed by the quark mass m over the nucleon mass M and the twist-3 term ξ which arises from quark-gluon correlations.

It is interesting to note that the quantity d_2 also appears in the first moment of g_1 when at large Q^2 ($Q^2 \gg \Lambda^2_{QCD}$) it is expressed in terms of a twist expansion [13, 12]:

$$\Gamma_1(Q^2) = \int_0^1 g_1(Q^2,x)dx = \frac{1}{2}a_0 + \frac{M^2}{9Q^2}\left(a_2 + 4d_2 + 4f_2\right) + O\left(\frac{M^4}{Q^4}\right), \quad (5)$$

where a_0 is the leading twist, dominant contribution. It is determined, apart from QCD radiative corrections [14], by the triplet g_A and octet a_8 axial charges and the net quark spin contribution to the total nucleon spin. These axial charges are extracted from measurements of the neutron and hyperons weak decay measurements [15]. Here a_2 is a second moment of the g_1 structure function and arises from the target mass correction [12]. The quantities d_2 and f_2 are the twist-3 and the twist-4 reduced matrix elements. These matrix elements contain non-trivial quark-gluon interactions beyond the parton model. A first extraction of f_2 has been carried by Ji and Melnitchouk in [16] using the world data but with poor statistical precision below Q^2 = 1 GeV^2. Other investigations of higher twist contributions in the case of spin-dependent structure

functions were performed and reported in Ref. [17, 18]. Recent extractions of f_2 separately for the neutron and the proton as well as the non-singlet combination $f_2^{p-n} = f_2^p - f_2^n$ have also been carried out combining the existing high Q^2 world data with new low Q^2 data from Jefferson Lab [19, 20, 21, 22]. The new data helped gauge the size of higher twist contribution (beyond twist-4), thus checking the convergence of the expansion, and providing for an improved precision in the extraction of f_2.

In QCD, d_2 and f_2 can be expressed as linear combinations of the induced color electric and magnetic polarizabilities χ_E and χ_B [8, 23] when a nucleon is polarized. This twist expansion may be valid down to $Q^2 \approx 1$ GeV^2 if higher order terms are small.

At large Q^2 where an OPE expansion becomes valid, the quantity d_2 reduces to a twist-3 matrix element which is related to a certain quark-gluon correlation.

$$d_2 S^{[\mu} P^{\{\nu]} P^{\lambda\}} = \frac{1}{8} \sum_q \langle P,S|\bar{\psi}_q \, g\widetilde{F}^{\{\mu\nu}\gamma^{\lambda\}}\psi_q|P,S\rangle \ , \tag{6}$$

where g is the QCD coupling constant, $\widetilde{F}^{\mu\nu} = (1/2)\varepsilon^{\mu\nu\alpha\beta}F_{\alpha\beta}$, $F_{\alpha\beta}$ are the gluon field operators, and the parentheses $\{\cdots\}$ and $[\cdots]$ denote symmetrization and antisymmetrization of indices, respectively. The structure of the above operator suggests that it measures a quark *and* a gluon amplitude in the initial nucleon wavefunction [6, 7].

The twist-4 contribution is defined by the matrix element

$$f_2 \, M^2 S^\mu \ = \ \frac{1}{2} \sum_q e_q^2 \, \langle P,S|g \, \bar{\psi}_q \, \widetilde{F}^{\mu\nu}\gamma_\nu \, \psi_q|P,S\rangle \ , \tag{7}$$

where $\widetilde{F}^{\mu\nu}$ is the dual gluon field strength tensor. f_2 can also be defined (generalized) in terms of the structure functions:

$$f_2(Q^2) = \frac{1}{2}\int_0^1 dx \, x^2 \Big(7g_1(x,Q^2) + 12g_2(x,Q^2) - 9g_3(x,Q^2) \Big), \tag{8}$$

where g_3 is the 3rd spin structure function, which has not yet been measured but could be accessed by an asymmetry measurement of unpolarized lepton scattering off a longitudinally polarized target. With only g_1 and g_2 data available, f_2 can also be extracted through Eqn. 5 if the twist-6 or higher terms are not significant.

The physical significance of $d_2(Q^2)$ has been articulated by Ji and we quote,

> *[W]e ask when a nucleon is polarized in its rest frame, how does the gluon field inside of the nucleon respond? Intuitively, because of the parity conservation, the color magnetic field $\vec{B}$ can be induced along the nucleon polarization and the color electric field $\vec{E}$ in the plane perpendicular to the polarization.*

After introducing the color-singlet operators $O_B = \psi^\dagger g\vec{B}\psi$ and $O_E = \psi^\dagger \vec{\alpha} \times g\vec{E}\psi$, we can define the gluon-field polarizabilities χ_B and χ_E in the rest frame of the nucleon[10, 11]

$$\langle PS|O_{B,E}|PS\rangle = \chi_{B,E} 2M^2 \vec{S} \, . \tag{9}$$

Then d_2 can be written as

$$d_2 = (\chi_E + 2\chi_B))/8 \, . \tag{10}$$

Thus d_2 is a measure of the response of the color electric and magnetic fields to the polarization of the nucleon. The reduced matrix element f_2 can be expressed also as a different linear combination of the same color polarizabilities

$$f_2 = (\chi_E - \chi_B)/3 \, . \tag{11}$$

Ultimately the color electric and magnetic polarizabilities will be obtained from $d_2(Q^2)$ and $f_2(Q^2)$ when high precision data on both g_1 and g_2 become available. In this proposal we are aiming at mapping out the (x,Q^2) behavior of g_2 and providing significantly enhanced data for d_2^n at large Q^2.

2.2 Burkhardt-Cottingham Sum rule

The g_2 structure function itself obeys the Burkhardt-Cottingham (BC) sum rule [25]

$$\Gamma_2(Q^2) = \int_0^1 g_2(x,Q^2)\, dx = 0\ , \tag{12}$$

which was derived from the dispersion relation and the asymptotic behavior of the corresponding spin-flip Compton amplitude. This sum rule is true at all Q^2 and does not follow from the OPE. It is rather a super-convergence relation based on Regge asymptotics as articulated in the review paper by Jaffe [26]. Many scenarios which could invalidate this sum rule have been discussed in the literature [7, 27, 28]. However, this sum rule was confirmed in perturbative QCD at order α_s with a $g_2(x,Q^2)$ structure function for a quark target [29]. Surprisingly a first precision measurement of g_2 by the E155 collaboration [24] at Q^2 = 5 GeV^2 but within the experimentally limited range of x has revealed a violation of this sum rule on the proton at the level of three standard deviations. In contrast, the neutron sum rule is poorly measured but consistent with zero within one standard deviation. New high precision neutron g_2 data [30, 31] shown in Fig. 6 at Q^2 below 1 GeV suggest that the BC sum rule is verified within errors. While a full test of the BC sum rule cannot be performed within the limited x range of this proposal, this measurement will provide useful data to further explore the large x contributions to the sum rule in the neutron/^{3}He.

3 Experimental status of $d_2^{p,n}(Q^2)$ and $\Gamma_2^n(Q^2)$ measurements

The early measurements of the g_2 spin structure function performed by the SMC [32] and E142 [33, 34] collaborations in the 90's were meant to reduce the systematic errors when extracting g_1 due to g_2's contribution to the measured parallel asymmetries. As the statistical precision of g_1 improved, a better measurement of g_2 was required to minimize the error on g_1. Therefore, in SLAC E143 [35], E154 [36] and E155 [37] more data on g_2 were collected and d_2 was evaluated and published by these collaborations. But since the statistical errors of these experiments were still large and as the interest in the physics of g_2 rose, a dedicated experiment known as SLAC E155x [38] was approved to measure g_2 at relatively large Q^2 to investigate the higher twist effects in the proton and deuteron. This led to an evaluation of d_2 with much improved statistical precision compared to what existed previously for both the proton and the deuteron [38]. At lower Q^2 another dedicated experiment known as JLab E97-103 [40] was performed at Jefferson Lab to look for higher twists effects by exploring the Q^2 evolution of g_2^n using a polarized ^{3}He target from Q^2 = 1.4 GeV^2 down to Q^2 = 0.6 GeV^2 at x = 0.2. The statistical precision was improved by almost an order of magnitude. Two other JLab experiments, E99-117 [39] and E94-010 [30, 31], had the opportunity to measure the g_2 structure function in a non-dedicated mode while focusing on a measurement of the g_1^n structure function. The first one provided three data points in the valence quark DIS region (x, Q^2) = (0.33, 2.71), (0.47, 3.52) and (0.6, 4.83) while the second one was carried out in the resonance region at Q^2 below 1 GeV^2.

Fig. 3 shows d_2 from SLAC E155X for the proton in the upper panel and the SLAC E155x and JLab E99-117 combined neutron result compared to several calculations. The proton result is generally consistent with the chiral quark model [61, 46] and some bag models [47, 12, 16] while one to two standard deviations away from the QCD sum rule calculations [48, 49, 50]. More importantly, the comparison with the recent lattice QCD calculation of the QCDSF collaboration [51] shows consistency with the experimental datum of the proton. However, it clearly indicates the need for an improvement on the experimental precision for the neutron datum. In fact Jefferson Lab E99-117 measurements of g_2^n at large x combined with SLAC E155X have improved on the total error by almost a factor of two. At the same time the latest QCDSF lattice calculation reported here has improved also by a factor of two compared to their previous results published in 2001 [52]. Of course it is difficult to guess the total error on the lattice calculation but at this time the neutron d_2 result is two standard deviations away from the experimental value including the lattice and chiral extrapolation errors. The experimental error bar is still dominated by the statistical uncertainty.

The Lattice Hadron Physics Collaboration (LHPC) based at Jefferson Lab has plans to extract this matrix element for the proton and the neutron [53] and provides a different check on the QCDSF collaboration lattice calculations.

It is worth noting that, except for the QCD sum rule calculation, all nucleon bag models or chiral soliton models predict values consistent with the lattice QCD result. The experimental result is thus 2σ away from zero all available calculations. In these models g_2^n is negative at large x, therefore it is conceivable that the poor precision (Fig. 5) of the data in this region is affecting the overall sign of the result. It is important to note that from the point of view of a simple quark model, the d_2 matrix element of the neutron should be much smaller than that of the proton because of SU(6) spin-flavor symmetry. Thus, with the present precision of the combined SLAC E155x and JLab E99-117 neutron data it is difficult to draw any conclusions on the sign and size of the neutron higher twist (twist-three) contribution. However because d_2 is a second moment in x of the linear combination $(2g_1 + 3g_2)$ the neutron data set can be improved significantly at Jefferson Lab with a dedicated measurement like the one proposed here. Due to the x^2 weighting, the contribution of the small x region is suppressed and thus using the existing world data to cover the region $x < 0.23$ should be sufficient to complete the integral.

During JLab experiment E94-010 [30], which was aimed at measuring the Gerasimov-Drell-Hearn extended sum, data on g_2 were taken using a polarized ^{3}He target across the resonance in the range $0.1 < Q^2 < 0.9$ GeV^2. New results on two moments of the neutron spin structure functions, Γ_2^n and d_2^n, are now avail-

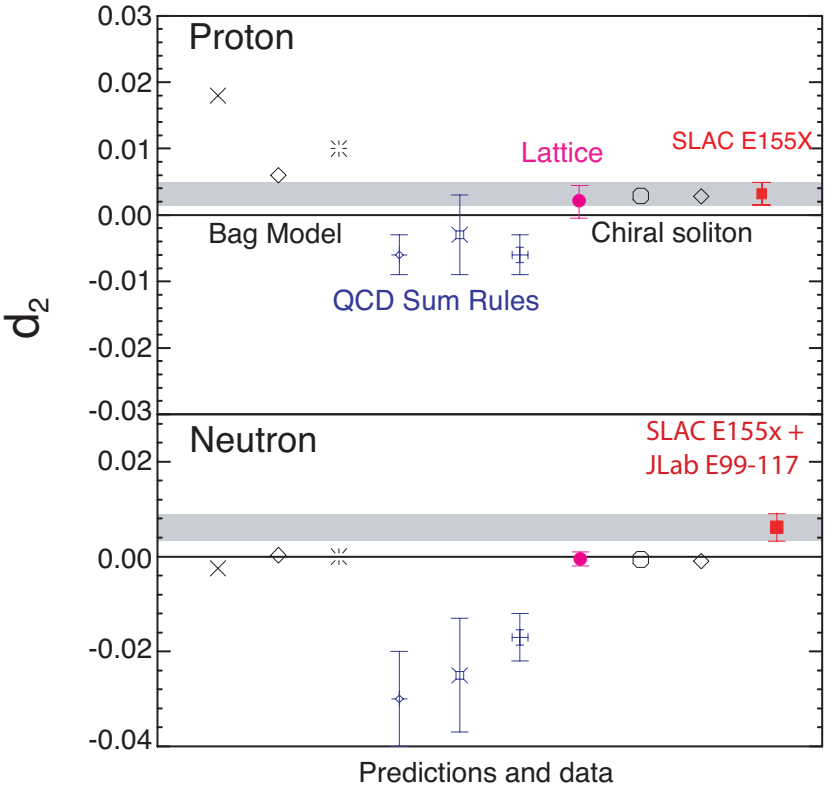

Figure 3: d_2 SLAC E155X results of the proton and SLAC E155x combined with JLab E99-117 results of the neutron results compared to several theoretical calculations including lattice QCD (see text). Upper panel is for the proton and lower panel is for the neutron.

able from this experiment. These low Q^2 results are shown in Fig. 4 along with the SLAC E155x and JLab E99-117 combined results. The results published in [31] give a glimpse of the Q^2 evolution of the quantity $\bar{d}_2^n$ which does not include the elastic contribution (at $x = 1$) to the integral. However this contribution is negligible above Q^2= 3 GeV^2 but dominate the quantity d_2 below Q^2 = 1 GeV^2. Note that no comparable data exist for the proton.

In the investigation of higher twists contributions an important step has already been taken with JLab experiment E97-103 [40], which has provided precision data of g_2^n in the deep inelastic region and determined its Q^2 evolution in the range $0.56 < Q^2 < 1.4$ GeV^2 for a fixed value of $x \approx 0.2$. The unprecedented statistical accuracy achieved in JLab E97-103 was critical to probe the size of higher twists contributions by comparing directly the measured g_2^n to the leading twist contribution (the twist-two contribution known as $g_2^{n(WW)}$ [42]). The experiment has been completed and the results published [40] showing a small but finite size of higher twists as Q^2 decreases below 1 GeV^2. However, as the coverage was in the low-x region, this experiment has little impact on the evaluation of the d_2 integral. Note that this does not diminish its importance for direct comparison between the measured g_2 and the leading twist piece of g_2.

Two other recently completed experiments, JLab experiment E01-012 [43] which used a polarized ^{3}He target, and JLab experiment E01-006 [44] which uses polarized NH_3 and ND_3 targets, will add to the wealth of neutron spin structure functions data (g_1^n and g_2^n) in the resonance region. However, the first measurement emphasizes the investigation of g_1 while the second provides data at Q^2 = 1.3 GeV^2 for g_2^p

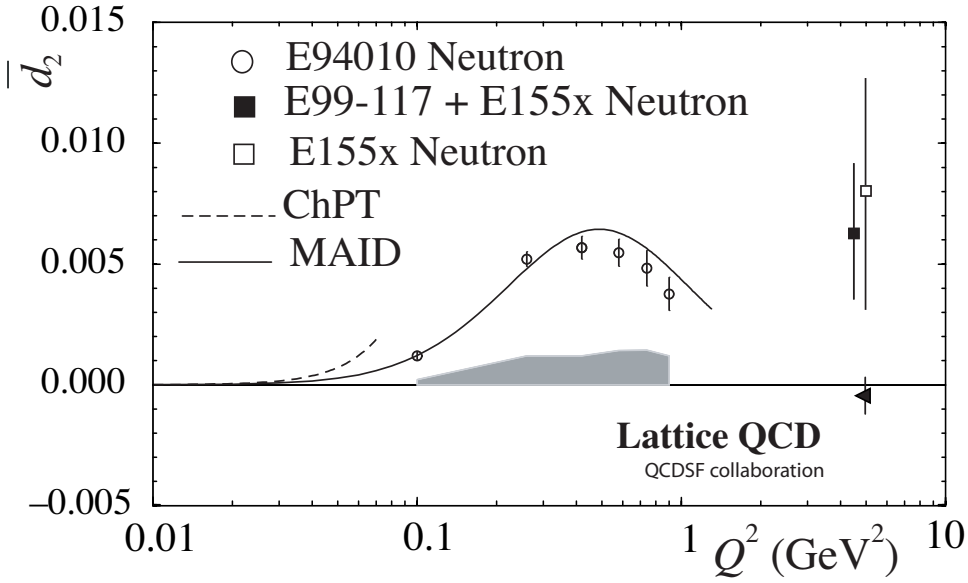

Figure 4: $\bar{d_2}(Q^2)$ results of JLab E94-010 without the nucleon elastic contribution are presented. The grey band represents their corresponding systematic uncertainty. The SLAC E155 [38] neutron result is also shown here (open square). The solid line is the MAID calculation[55] while the dashed line is a HBχPT calculation[56] valid only at very low Q^2. The lattice prediction [51] at Q^2 = 5 GeV^2 for the neutron d_2 reduced matrix element is negative but consistent with zero. We note that all models shown in Fig. 3 predict a negative value or zero at large Q^2 where the elastic contribution is negligible. At moderate Q^2 the data show a positive $\bar{d_2^n}$, and indicate a slow decrease with Q^2. The combined SLAC+JLab datum shows a positive d_2^n value but with still a large error bar.

with high precision but limited precision for g_2^n.

We summarize the situation of the quality of the neutron g_2 spin structure data in Fig. 5 where we report the world data with Q^2 greater than 1 GeV^2, the projected results of the approved JLab experiment E06-014, and show a comparison with some model calculations as well as the Wandzura-Wilczek g_2^{WW} contribution to g_2. The neutron g_2 extracted from the proton and deuteron measurements of E155X are also shown. The statistical accuracy already achieved in JLab E97-103 is displayed for their highest Q^2 kinematics point at $Q^2 = 1.4\,\mathrm{GeV}^2$, $x = 0.2$.

The proposed measurement is optimized to minimize the error on the determination of g_2^n. Obviously, the ultimate statistical precision at each x value will help for stringent comparison with models of $g_2^n(x, Q^2)$.

Finally, turning to the BC sum rule, the experimental situation is summarized in Fig. 6 where we show Γ_2^n measured in E94-010 (solid circles) and, including the elastic contribution (open circles) evaluated using a dipole form factor for G_M^n and the Galster fit for G_E^n. The positive light grey band corresponds to the total experimental systematic errors while the dark negative band represents an estimated DIS contribution using g_2^{WW}. The solid line is the resonance contributions evaluated using MAID and the negative light-grey band is the neutron elastic contribution added to the measured data to determine Γ_2^n. The results are quite encouraging since the data show that the BC sum rule is verified within uncertainties over the Q^2 range measured. Our result is at odds with the reported violation of this sum rule on the proton at high Q^2 (where the elastic contribution is negligible) [24]. It is, however, consistent with the neutron result of SLAC E155 (open square) which unfortunately has a rather large error bar. In light of our results, a high statistical

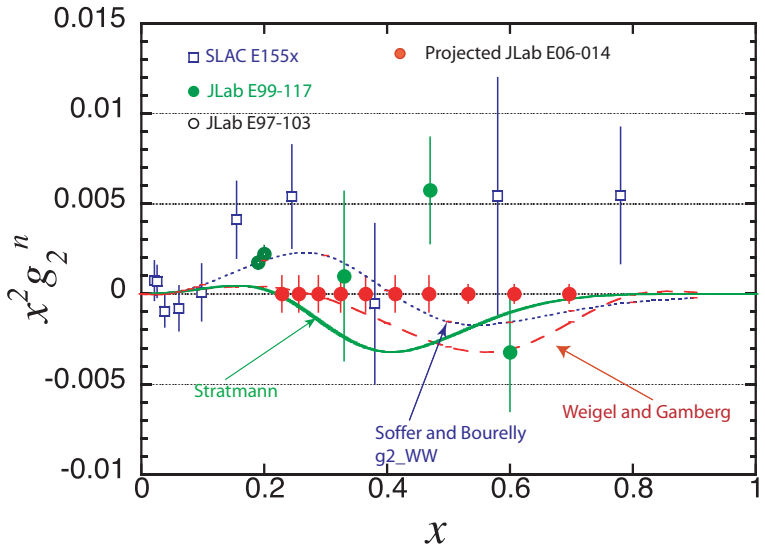

Figure 5: Present world $x^2 g_2^n$ data for $Q^2 \geq 1$ GeV^2 along with some model calculations and g_2^{WW}. SLAC E155X neutron results are derived from measurements using polarized NH_3 and ND_3 targets as described in Ref.[41, 24]. The JLab experiments used a polarized ^{3}He target in Hall A. We note the consistency between the data. The solid curve is a quark model calculation by Stratmann [47], the dashed line is a chiral soliton calculation by Weigel and Gamberg [61]. The dotted line represent the evaluation of g_2^{WW} using g_1 from the statistical model of the nucleon by Bourelly and Soffer [54].

precision measurement in the range 1 GeV$^2 \leq Q^2 \leq 5$ GeV^2 would be very useful for both the proton and neutron even if the x range is limited.

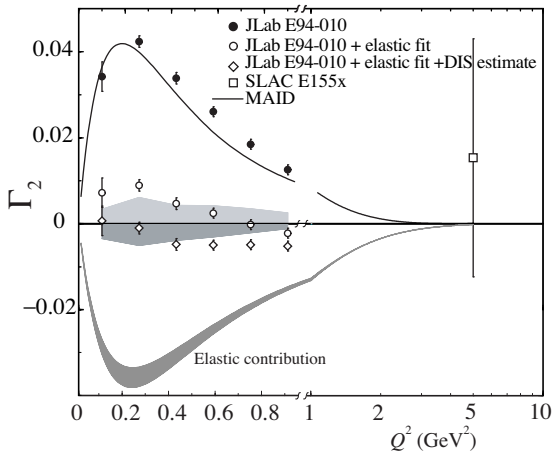

Figure 6: Results of Γ_2^n (open diamonds) along with the average of the world data from DIS. The theoretical prediction for this quantity is zero (see text).

In the next section we shall describe how we plan to improve on the statistical precision of the g_2 neutron data at large x which, when combined with the anticipated E06-014 results, will result in a reduction of the

statistical error bar of d_2^n by a factor of almost four as well as provide a reasonable add-on to the d_2^n and BC sum evaluations at $< Q^2 >$ = 3 and 4 GeV^2.

4 Proposed Experiment

We propose to measure the unpolarized cross section $\sigma_0^{^3He}$, the parallel asymmetry $A_{\|}^{^3He}$ and the perpendicular asymmetry $A_{\perp}^{^3He}$ to extract the g_2 structure function in the large x region with good precision. We will use the longitudinally polarized (P_b = 0.80) CEBAF electron beam and a 40 cm-long high pressure polarized ^{3}He target. The measurement will be performed using two kinematic configurations:

- E_{beam} = 8.8 GeV, with the spectrometers at $\theta = \pm 30.0^\circ$
- E_{beam} = 6.6 GeV, with the spectrometers at $\theta = \pm 40.0^\circ$

At each beam energy the BigBite spectrometer will be used to acquire the asymmetry data (perpendicular and parallel) while the left arm HRS spectrometer will be used to measure the absolute cross section. Both spectrometers will be set at equal scattering angles to each side of the incident beam line (Fig. 7). BigBite's mode of operation is such that a single magnetic field setting will cover the entire kinematic range at each beam energy. The left HRS momentum will be stepped across the same kinematic range to measure the absolute cross section as a function of x. The target polarization orientation will be set transverse or longitudinal to the beam with a value of P_t = 0.50 while the beam helicity will be reversed at a rate of 30 Hz. A beam current of 10 μA combined with a 30 cm target (after cuts) of density 10 amg provides a luminosity of 5×10^{35} cm^{-2}s^{-1}.

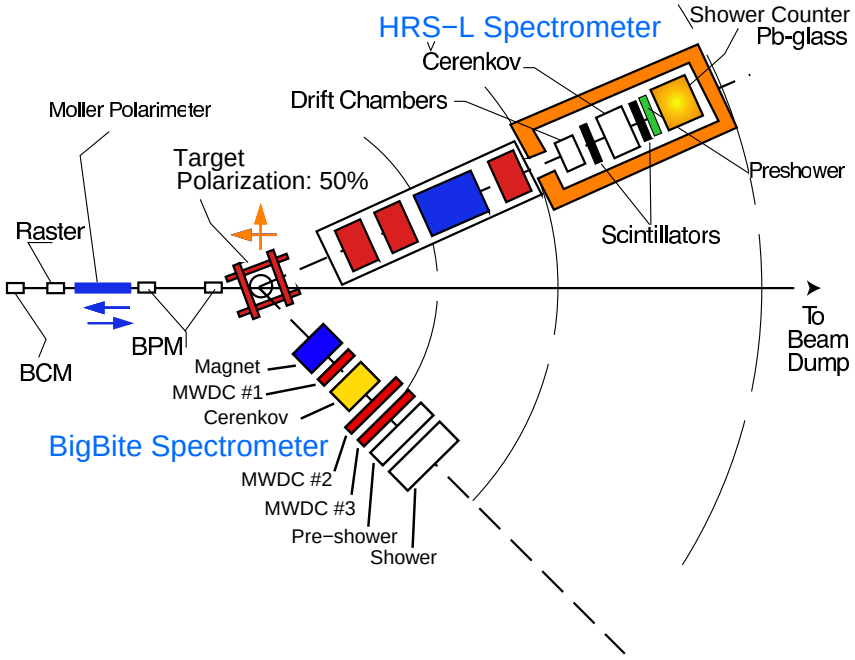

Figure 7: Diagram of floor layout for this proposal showing BigBite and the LHRS at equal angles on either side of the beamline.

4.1 Choice of Kinematics

The kinematics for this experiment were optimized in such a way that the the matrix element d_2^n can be extracted at large Q^2 and large x in a reasonable amount of running time. The data will be complementary to those of the approved 6.0 GeV experiment E06-014. The combined data will allow us to make a confident

evaluation of the Q^2 evolution of g_2^n for $0.5 < x < 0.7$. The x-range will be limited by the 6 GeV cut-off in x. In addition, d_2^n will be evaluated for different values of Q^2. We plan to extract g_1^n and g_2^n by measuring parallel and perpendicular asymmetries. The directions are defined relative to the momentum of the incoming electron beam.

The usual method of extracting the spin structure functions is to use the following relationships for the asymmetries:

$$A_{\parallel} = \frac{1}{F_1(x,Q^2)} \frac{1-\varepsilon}{\nu(1+\varepsilon R(x,Q^2)} (g_1^n(E+E'cos(\theta)) - \frac{Q^2}{\nu} g_2^n), \tag{13}$$

$$A_{\perp} = \frac{1}{F_1(x,Q^2)} \frac{1-\varepsilon}{\nu(1+\varepsilon R(x,Q^2)} E'sin(\theta)(g_1^n + \frac{2E}{\nu} g_2^n). \tag{14}$$

Using Eqns. 13 and 14 for the extraction of g_1^n and g_2^n relies on the knowledge of the unpolarized structure function $F_1^n(x,Q^2)$. This structure function is related to $F_2^n(x,Q^2)$ (via the Callan-Gross relation) and has been measured over a large kinematic range. A variety of existing parton distribution functions can be used to reproduce the F_2^n structure function well. At large values of Q^2 and x the nucleon resonances disappear and global (and local) Bloom-Gilman duality is well established.

However, another technique exists that is considerably more direct and provides a cleaner method of extracting the spin structure functions. The addition of the unpolarized cross section measurement taken simultaneously by the LHRS to the asymmetry measurements from BigBite allow the direct extraction of g_1^n and g_2^n through the following expressions:

$$g_1 = \frac{MQ^2}{4\alpha^2} \frac{y}{(1-y)(2-y)} 2\sigma_0 \left[A_{\parallel} + \tan\frac{\theta}{2} A_{\perp} \right] \tag{15}$$

$$g_2 = \frac{MQ^2}{4\alpha^2} \frac{y^2}{2(1-y)(2-y)} 2\sigma_0 \left[-A_{\parallel} + \frac{1+(1-y)\cos\theta}{(1-y)\sin\theta} A_{\perp} \right] \tag{16}$$

where σ_0 is the unpolarized cross section, Q^2 is the four momentum transfer, α the electromagnetic coupling constant, θ the scattering angle and $y = (E-E')/E$ the fraction of energy transferred to the target. $A_{\parallel}$ and $A_{\perp}$ are the parallel and perpendicular asymmetries,

$$A_{\parallel} = \frac{\sigma^{\downarrow\Uparrow} - \sigma^{\uparrow\Uparrow}}{2\sigma_0}, \qquad A_{\perp} = \frac{\sigma^{\downarrow\Rightarrow} - \sigma^{\uparrow\Rightarrow}}{2\sigma_0} \tag{17}$$

The quantity d_2 is obtained from the measurement of the linear combination of the spin structure functions $g_1(x,Q^2)$ and $g_2(x,Q^2)$ and forming the second moment of this combination:

$$d_2(Q^2) = \int_0^1 x^2 [2g_1(x,Q^2) + 3g_2(x,Q^2)]\, dx = \int_0^1 \tilde{d_2}(x,Q^2)\, dx \tag{18}$$

Equations 15, 16, and 17 are then used to rewrite the integrand of d_2 directly in terms of measured asymmetries and the unpolarized cross section:

$$\tilde{d_2}(x,Q^2) = x^2[2g_1(x,Q^2) + 3g_2(x,Q^2)] \tag{19}$$

$$= \frac{MQ^2}{4\alpha^2} \frac{x^2y^2}{(1-y)(2-y)} \sigma_0 \left[\left(3\frac{1+(1-y)\cos\theta}{(1-y)\sin\theta} + \frac{4}{y}\tan\frac{\theta}{2} \right) A_{\perp} + \left(\frac{4}{y} - 3 \right) A_{\parallel} \right] \tag{20}$$

Table 1: Parameters used for rate estimates

kinematic setting	I	II
beam energy	6.6 GeV	8.8 GeV
beam current	10 μA	10 μA
beam polarization	0.80	0.80
scattering angle	40°	40°
momentum range	0.2 GeV $\rightarrow$ 2.37 GeV	0.2 GeV $\rightarrow$ 3.85 GeV
z-acceptance	0.2 m	0.2 m
solid angle	50 msr	50 msr
efficiency	0.67	0.67
eff. target length	30 cm	30 cm
target polarization	0.50	0.50
eff. target density	10.3 amg	10.3 amg

Table 2: Kinematic bins and expected rates for BigBite setting I. The uncertainties for $A_{\parallel}$ and $A_{\perp}$ are *statistical* only and are based on 25 hours ($\parallel$) and 175 hours ($\perp$) of running time.

E_i [GeV]	E'_{cent} [GeV]	Q^2 [GeV^2]	x	W [GeV]	e^- rate [Hz]	π^- rate [Hz]	$dA_{\parallel}$	$dA_{\perp}$
6.6	1.041	3.213	0.308	2.849	16.3	1189	$9.2 \cdot 10^{-4}$	$3.5 \cdot 10^{-4}$
6.6	1.199	3.702	0.365	2.707	12.6	591.7	$1.0 \cdot 10^{-3}$	$4.0 \cdot 10^{-4}$
6.6	1.357	4.191	0.426	2.558	9.3	257.1	$1.2 \cdot 10^{-3}$	$4.6 \cdot 10^{-4}$
6.6	1.516	4.680	0.490	2.399	6.5	98.0	$1.5 \cdot 10^{-3}$	$5.5 \cdot 10^{-4}$
6.6	1.674	5.169	0.559	2.229	4.1	32.8	$1.8 \cdot 10^{-3}$	$6.9 \cdot 10^{-4}$
6.6	1.832	5.658	0.632	2.045	2.3	9.7	$2.4 \cdot 10^{-3}$	$9.2 \cdot 10^{-4}$
6.6	1.991	6.147	0.710	1.843	1.1	2.5	$3.6 \cdot 10^{-3}$	$1.4 \cdot 10^{-3}$
6.6	2.149	6.636	0.794	1.616	0.35	0.58	$6.3 \cdot 10^{-3}$	$2.4 \cdot 10^{-3}$
6.6	2.307	7.125	0.884	1.350	0.053	0.12	$1.0 \cdot 10^{-2}$	$6.1 \cdot 10^{-3}$
6.6	2.466	7.614	0.981	1.018	0.003	0.021	$7.2 \cdot 10^{-2}$	$2.7 \cdot 10^{-2}$

4.2 Rates and Statistical Uncertainties

The rates and statistical uncertainties were estimated using the parameters listed in Table 1. The parametrization MRST2001LO [1] for parton distribution functions was used to construct the unpolarized structure functions. The range of validity of this parametrization is estimated to be $1.0 \times 10^{-5} \leq x \leq 1.0$ and $1.25 \leq Q^2 \leq 1.0 \times 10^7$. Two additional parametrizations (CTEQ61 [2] and H12000LO [3]) were used to study the variations in the counting rates (it was checked for one kinematic setting). The agreement was better than 10%. Table 2 summarizes the proposed binning and expected rates for kinematic setting I. Note that this corresponds to a single spectrometer setting for BigBite and 10 settings for the HRS. The BigBite coverage will be divided into 10 matching momentum bins offline. Table 3 shows the expected rates for kinematic setting II. As with the 6.6 GeV kinematics, this corresponds to a single spectrometer setting for BigBite and 10 settings for the HRS. The BigBite momentum bite will be divided into 10 matching momentum bins offline.

Figure 8 plots the BigBite (x, Q^2) coverage for the two kinematics. The colored subdivisions within each kinematic stripe reflect how the BigBite data will be divided into bins offline. The HRS kinematics are

Table 3: Kinematic bins and expected rates for BigBite setting II. The uncertainties for $A_{\parallel}$ and $A_{\perp}$ are *statistical* only and are based on 40 hours ($\parallel$) and 360 hours ($\perp$) of running time.

E_i [GeV]	E'_{cent} [GeV]	Q^2 [GeV^2]	x	W [GeV]	e^- rate [Hz]	π^- rate [Hz]	$dA_{\parallel}$	$dA_{\perp}$
8.8	1.111	2.621	0.182	3.565	55.9	7429	$5.3 \cdot 10^{-4}$	$1.3 \cdot 10^{-4}$
8.8	1.412	3.328	0.240	3.382	44.3	2491	$5.4 \cdot 10^{-4}$	$1.4 \cdot 10^{-4}$
8.8	1.712	4.036	0.303	3.188	34.2	739.4	$5.7 \cdot 10^{-4}$	$1.6 \cdot 10^{-4}$
8.8	2.012	4.744	0.372	2.982	25.3	197.5	$6.2 \cdot 10^{-4}$	$1.9 \cdot 10^{-4}$
8.8	2.312	5.452	0.448	2.761	17.4	48.0	$7.2 \cdot 10^{-4}$	$2.3 \cdot 10^{-4}$
8.8	2.612	6.160	0.530	2.520	10.7	10.7	$8.7 \cdot 10^{-4}$	$3.0 \cdot 10^{-4}$
8.8	2.912	6.867	0.621	2.254	5.5	2.2	$1.2 \cdot 10^{-3}$	$4.2 \cdot 10^{-4}$
8.8	3.213	7.575	0.722	1.951	2.0	0.4	$1.9 \cdot 10^{-3}$	$7.0 \cdot 10^{-4}$
8.8	3.513	8.283	0.834	1.592	0.48	0.07	$4.3 \cdot 10^{-3}$	$1.6 \cdot 10^{-3}$
8.8	3.813	8.991	0.960	1.124	0.005	0.01	$3.7 \cdot 10^{-2}$	$1.5 \cdot 10^{-2}$

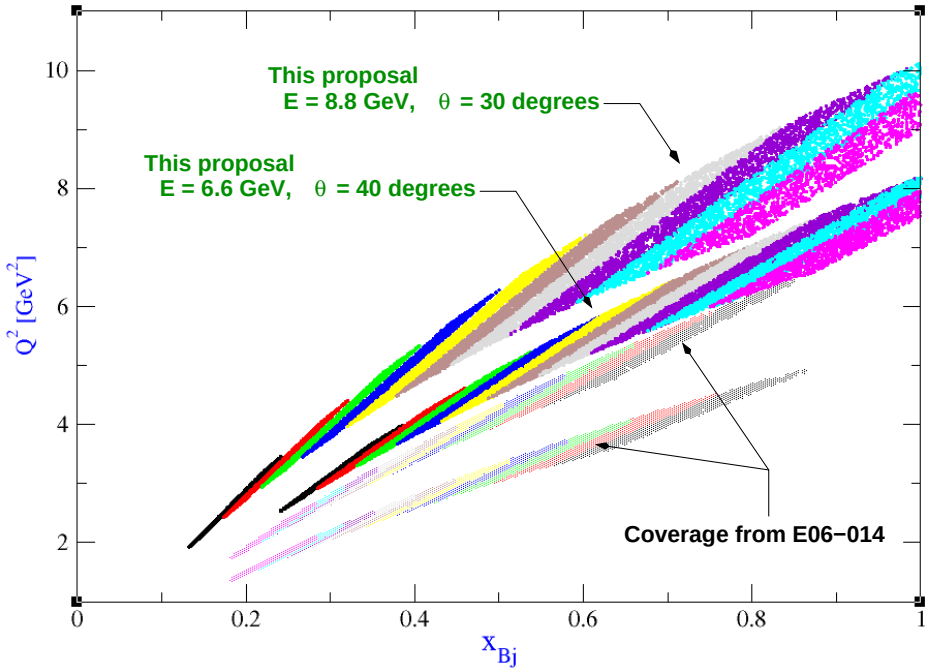

Figure 8: The two upper stripes reflect the BigBite (x, Q^2) coverage for the proposed measurement at 6.6 and 8.8 GeV. The colored subdivisions within each kinematic stripe reflect how the BigBite data will be divided into bins offline. The HRS kinematics are chosen to match the central (x, Q^2) value for each of those bins. The lower stripes reflect the coverage from the lower energy measurement E06-014.

chosen to match the central (x, Q^2) value for each of those bins. The lower stripes reflect the coverage from E06-014 which will run in early–2008.

The electron rates quoted in Tables 2 and 3 are the rates from ^{3}He only. Additional rates from small admixtures of the buffer gas nitrogen were checked and can be neglected. Scattering from the end windows will be minimized using software cuts.

The parallel vs. perpendicular running times were estimated in two independent ways: i) minimization of the statistical uncertainty in g_2^n, and ii) minimization of the statistical uncertainty in $x^2(2g_1 + 3g_2)$. Both methods yielded essentially the same time distribution. The requested beamtime includes 200 hours for the 6.6 GeV kinematics, 400 hours for the 8.8 GeV setting, and an additional 100 hours for calibration and overhead. The total is 700 hours, or roughly 29 days of beam.

4.2.1 Positron Contamination

Another source of background are electrons from e^+/e^- pair creation. We assumed the positrons are generated from Dalitz decays of π^0's and conversion of decay photons in the target and materials surrounding the target. The positrons are then detected in the spectrometer. A reasonable approximation for this background estimate is taking the average of π^- and π^+ rates [4]. The cross sections were obtained from fits by D. Wiser [5]. Our lowest momentum bin will be limited by the (measured) e^-/e^+ ratio. We anticipate this limit to be around $x \approx 0.2$. We believe that we can easily resolve electron/positron pairs given the good spacial (angular) resolution of BigBite. The events can be removed via software cuts. Measurement of the positron production cross section during JLab E99-117 shows that it is less than 3% of the total cross section at $x = 0.33$ and scattering angle of 35°. In any case, we plan to measure the positron Cross sections by reversing the field in the left HRS to confirm our procedures.

5 Description of the Hardware

5.1 The Polarized Beam

In this proposal we shall assume that the achievable beam polarization at CEBAF is 80% with a current of $10\mu A$. The polarization of the beam will be measured with the Hall A Moller and Green Compton polarimeters.

The impact of radiation and heat load on the target cells will be minimized by using the raster system to steer the beam through a circular pattern with a diameter appropriate to the target dimensions.

5.2 The Green Compton Polarimeter

The electron beam polarization can be measured in Hall A using Compton polarimetry. Because the Compton scattering asymmetry can be calculated exactly in Quantum Electro-Dynamics (QED), the electron beam polarization can be extracted from the scattering asymmetry between the electron beam and a high power laser. The current Compton Polarimeter in Hall A utilizes a Fabry-Perot cavity operating at 1064 nm (IR) laser with about 1.5 kW of intra-cavity power. Both scattered electrons and photons are detected and the beam polarization is extracted from the measured asymmetry of either electron-only events or electron-photon coincidence events. The figure of merit (FOM, $\sigma\langle A\rangle^2$) is proportional to $k^2 \times E^2$ with k the photon energy and E the electron beam energy. The present polarimeter provides a systematic uncertainty of about 3% for a 4 GeV beam.

Over the next a few years there are a few experiments approved to run in Hall A which require higher precision. To meet the requirement of these experiments, an upgrade is being planned [80]. In it, the existing Fabry-Perot cavity will be replaced by a 532 nm (green) cavity with twice the power, resulting in a four-fold

enhancement of the FOM for the Compton polarimeter. Associated improvements to the electron detector, the photon calorimeter, and data acquisition method are also required. These upgrades are expected to be complete within the next couple of years and are crucial for both the upcoming experiments at 6 GeV and future experiments after the 12 GeV Upgrade. For an 11 GeV beam, Once the magnetic chicane has been upgraded to support an 11 GeV beam, it should be possible to achieve better than 1.5% absolute accuracy for the measured beam polarization.

One author of this proposal is already heavily involved in the Compton upgrade which is on-going at the Green Compton Polarimetry Lab in Jefferson Lab's ARC building. We expect to continue this effort and make significant contributions to the Green Compton development and commissioning at both 6 and 12 GeV.

5.3 The Polarized ^{3}He Target

The polarized ^{3}He target at JLab is based on optical pumping of a vapor of alkali atoms and subsequent spin exchange between the polarized atoms and the ^{3}He nuclei.

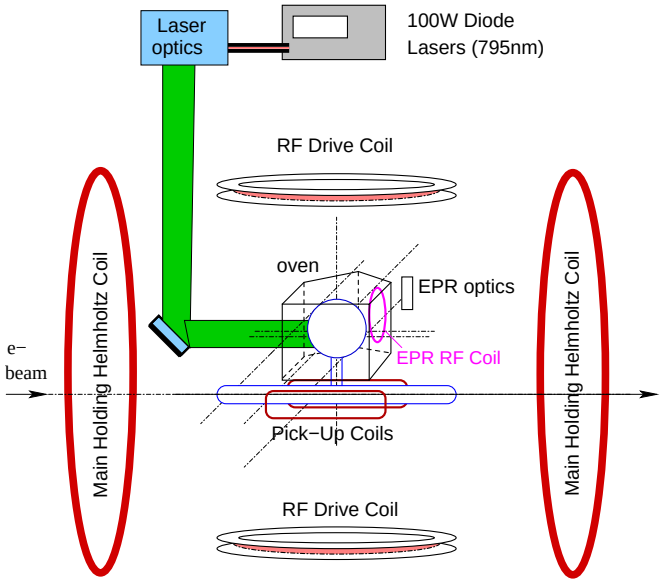

Figure 9: Typical layout of a polarized ^{3}He target. Note that for simplicity, only one of the three sets of orthogonal Helmholtz coils shown.

Figure 9 shows the basic layout of the polarized ^{3}He target which currently exists for research in Hall A [74]. The target holding field is provided by two sets of Helmholtz coils oriented normal to each other, hence the target spin direction can be aligned either parallel or perpendicular to the electron beam. Fig. 10 shows a picture of a standard 40 cm long cell. The cells for these experiments consist of a two chamber design. The upper spherical chamber contains the alkali vapor while the lower chamber is used for electron scattering from the polarized ^{3}He.

Approximately 100 Watts (total) of light from a set of 3-4 diode lasers is combined using an optical fiber coupler and directed through a series of optics to produce circularly polarized light at a wavelength of ~ 795 nm. This light is used to polarized the alkali vapor through optical pumping. The polarized alkali transfers its spin to the ^{3}He nuclei through collisions.

This target has been used by seven experiments in Hall A from 1998 to 2006 and is currently being re-designed for a series of five experiments planned for 2007 as shown in Figure 11. In addition to adding a

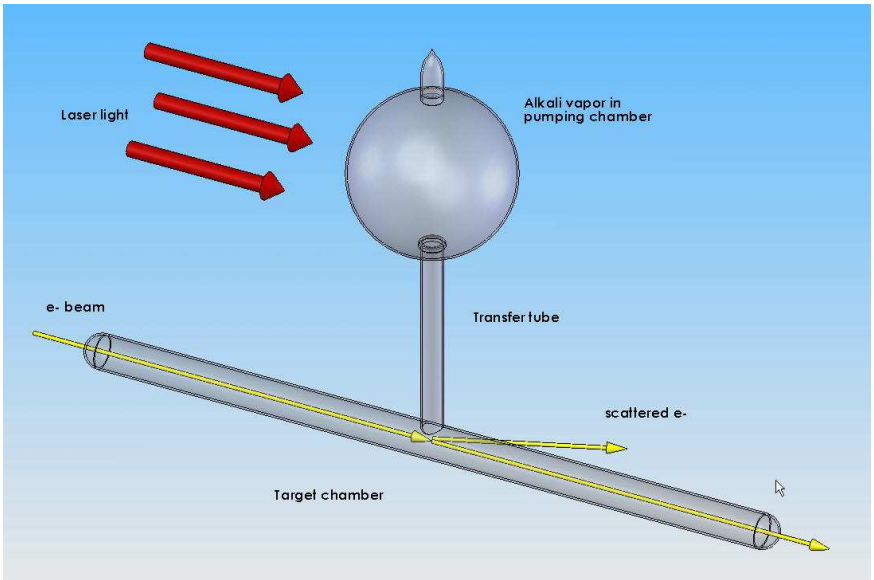

Figure 10: A standard polarized ^{3}He target cell. The cell consists of a spherical "pumping chamber," a cylindrical "target chamber," and a "transfer tube" connecting the two chambers. The electron beam passes through the 40 cm long target chamber as shown.

third set of Helmholtz coils to allow for polarization in the vertical direction, the new system will incorporate new design features allowing it to capitalize on the recent success of a similar target used for experiment E02-013 [75]. So-called 'hybrid' target cells [76] containing a mixture of potassium and rubidium were used to achieve over 50% polarization with 8 μA of beam current. During E02-013 a single cell was used with a beam current of 8 μA for 6 weeks without rupturing. Beam currents up to 15 μA could be used with a degradation in polarization and cell lifetime.

The target polarization can be measured using two methods: NMR and EPR (Electron-Paramagnetic Resonance). Each type of polarimetry can provide a relative 3% precision. In this document we use a polarization of 50% to estimate the expected uncertainties and beam time request. With a beam current of 10 μA and a typical target density of 12 amg under operating conditions, this provides a $e-\vec{n}$ luminosity of 5×10^{35} s^{-1} cm^{-2}.

This target continues to be a flagship facility for the Hall A program and will be relatively easy to adapt for use at 11 GeV in Halls A and C. Polarized target groups at the College of William and Mary and the University of Virginia continue to produce target cells with consistently-improving polarization. Through the combined effort of these groups and the polarized target groups and personnel at the University of Kentucky, Temple University, Duke University and Jefferson Lab this collaboration has the necessary experience and manpower for this polarized target system.

5.4 The Spectrometer Configurations

We plan to use the BigBite spectrometer in Hall A to take the bulk of the data, and one HRS spectrometer, the left arm, to perform cross section measurements and calibrations.

5.4.1 The BigBite spectrometer

BigBite is a non-focusing large momentum and angular acceptance spectrometer that was originally designed and built for use at the internal target facility of the AmPS ring at NIKHEF [77, 78]. The spectrom-

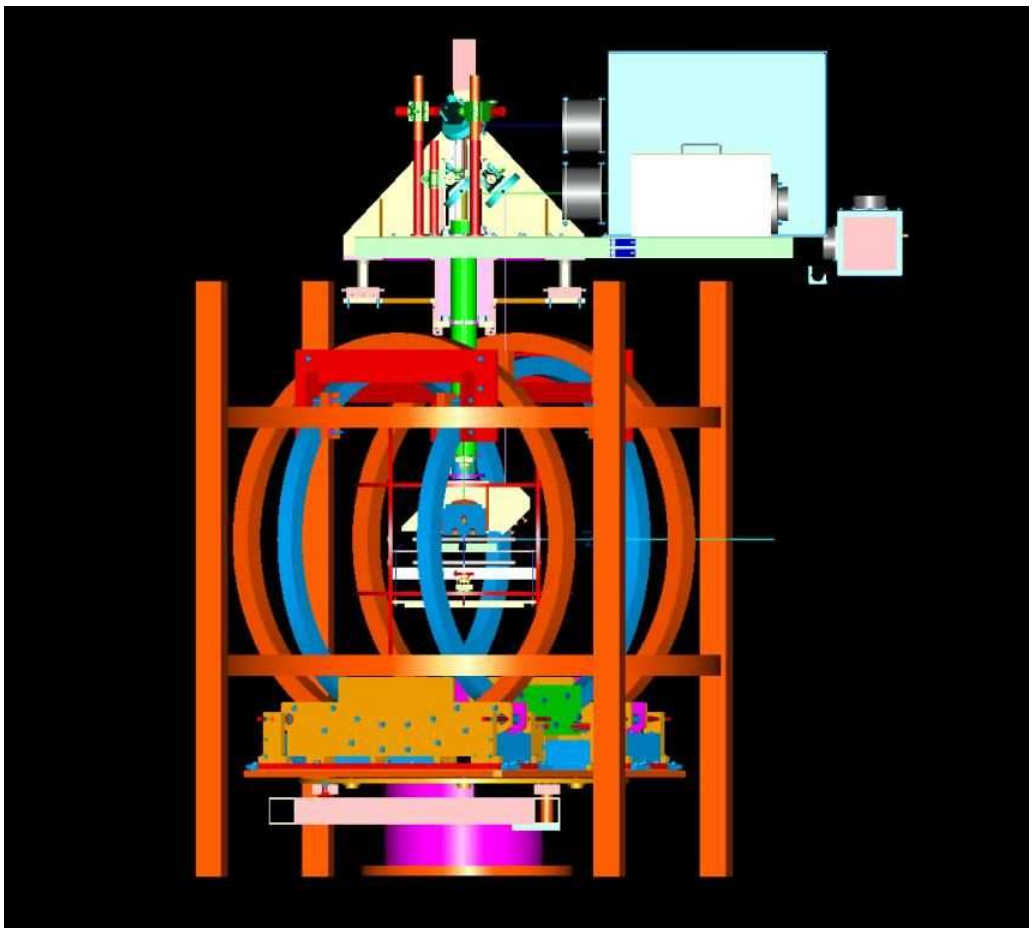

Figure 11: Current design (side view) of the Hall A polarized target system for the series of experiments planned for 2007-08. It is expected that this target system can be used with little modification for the 11 GeV programs in Halls A and C. Though the target itself is well-suited for use in Hall A or C, a new mounting system at the pivot, and accommodations for the lasers, will be needed for use in Hall C.

eter consists of a single dipole magnet (maximum magnetic field 1.2 Tesla) and a detection system. The original detector package included two sets of multi-wire drift chambers (MWDC), a plastic scintillator and an aerogel Cerenkov detector. Since the arrival of the BigBite spectrometer in Hall A, a series of highly rated experiments has been approved to use this powerful device. These experiments include the recently completed Hall A G_{E_n} experiment (E02-013), E04-007, E05-009, E05-015, E06-010, E06-011, and E06-014. To meet the high rate and high resolution requirements of these experiments a new detector package for BigBite was constructed. This detector package includes:

- Three Multi-wire Drift Chambers (MWDC) for tracking.
- A Gas Cerenkov counter for pion rejection.
- A double layer lead glass calorimeter for triggering on high energy electrons and for pion rejection.
- A plane of scintillators.

The set of MWDC, calorimeter and the scintillators were successfully used during the G_{E_n} experiment, with the raw rates on the MWDC as high as 20 MHz per plane. The Gas Cerenkov counter is being designed now

to be used for the neutron d_2 experiment (E06-014) which is scheduled to run in early 2008.

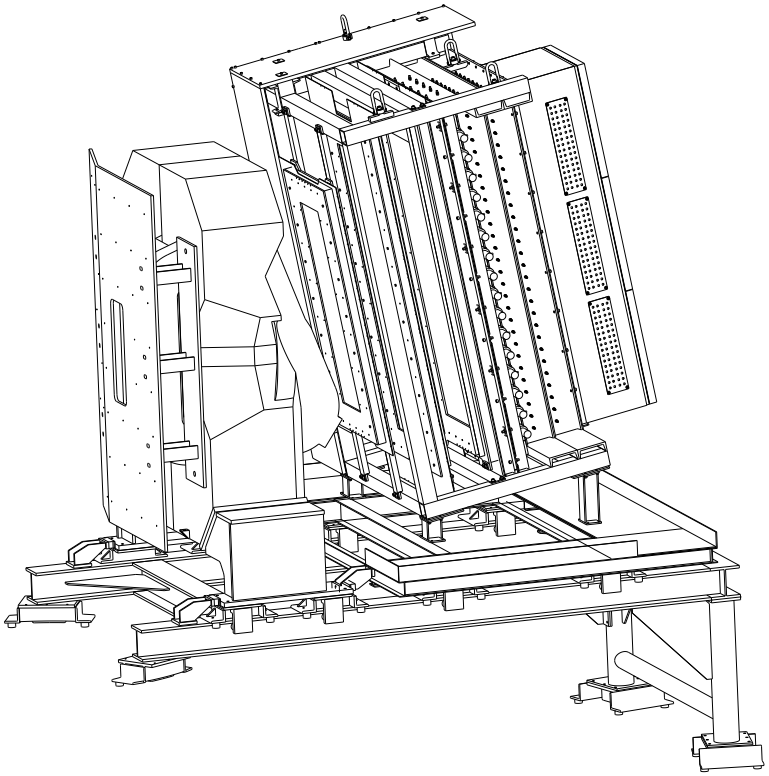

Figure 12: An overview of the BigBite spectrometer with the G_{E_n} detector package. Shown (from left to right) are the bending magnet (B_{max}=1.2 T), three MWDCs, the scintillator plane and the shower and pre-shower detectors. A Gas Cerenkov counter will be added to enhance the pion rejection capabilities.

To first order, the momentum of an electron detected by the BigBite spectrometer is inversely proportional to the deflection angle ($\theta_{\rm def}$) through the spectrometer. This was clearly verified in the G_{E_n} experiment where the momentum was found to follow the empirical relationship

$$P_e = \frac{(0.306 + 0.0189 x_{\rm bend})}{\theta_{\rm def}} + ... \tag{21}$$

to the 1.5% level over more than 75% of the BigBite acceptance. As the sizes of the coefficients indicate, the correction based on $x_{\rm bend}$, ($x_{\rm bend} < 0.5\,{\rm m}$) (the position of the track at the bend plane of the spectrometer) is at the 5% level.

For the G_{E_n} experiment, the BigBite spectrometer was located at 50°, 1.1 m from the target and the distance between the first and the third MWDC was 0.7 m. The limiting factor on luminosity for this experiment was the high rate of low energy particle hits in the MWDCs. As one would naïvely expect, the background rate (and the resulting MWDC current drain) dropped as the beam energy increased. During G_{E_n} the maximum operating currents for the 1.5 GeV and 2.6 GeV beam energies were 5.5 μA and 7 μA respectively. For 3.29 GeV running, the reduced background levels allowed us to increase the current to 8 μA. A GEANT simulation, normalized to G_{E_n} background rates, indicates that BigBite spectrometer located at 30°, 1.5 m from the target and 6 GeV Beam energy (conditions for the Hall A transversity experiment which is scheduled to run in late–2007) can be operated with beam currents up to 10.0 μA.

For the proposed measurement we plan to locate the BigBite spectrometer at 1.55 m from the target for 8.8 GeV beam energy running. Given the empirical evidence and simulation results above, we can expect

to be able to run at beam currents higher than 10 μA under these conditions. However, we are taking a conservative approach in this proposal and have assumed a 10 μA beam current for the rate estimates given here

The maximum momentum of the electrons detected in the G_{E_n} experiment was approximately 1.6 GeV. In the proposed experiment we plan to double the momentum reach of BigBite with electron momenta up to 3.2 GeV. As a result, the bend angles for these electrons will be about half of those for the G_{E_n} experiment. In order to account for this we will double the distance between MWDC #1 and MWDC #3 in the BigBite detector stack from 0.7 m to 1.4 m. This will approximately double the angular resolution, resulting in a 1.5% level momentum resolution for the 3.2 GeV electrons, similar to the resolution achieved for 1.6 GeV electrons in G_{E_n}. The increased resolution for the proposed setup has been verified using the BigBite GEANT simulation as indicated in the next section.

5.4.2 GEANT Simulation of BigBite

The package of programs for the simulation of the BigBite spectrometer characteristics was developed by V. Nelyubin [79]. The results from this simulation for the G_{E_n} configuration agreed very well with the momentum resolution and the solid angle acceptance achieved during the G_{E_n} experiment.

This simulation has been repeated for the conditions of the proposed experiment; electron momenta up to 3.5 GeV, BigBite located at 1.55 m from the target, and with the distance between the first and the third MWDC increased to 1.4 m. The results of this MC study of the BigBite momentum resolution are shown in Fig. 13, where the momentum resolution as a function of the electron momentum for a position resolution of 0.2 mm (the resolution of the MWDC) are plotted. The expected position resolution on target along the beam is σ= 5 mm, and the expected angular resolution in both scattering planes is σ=1 mrad.

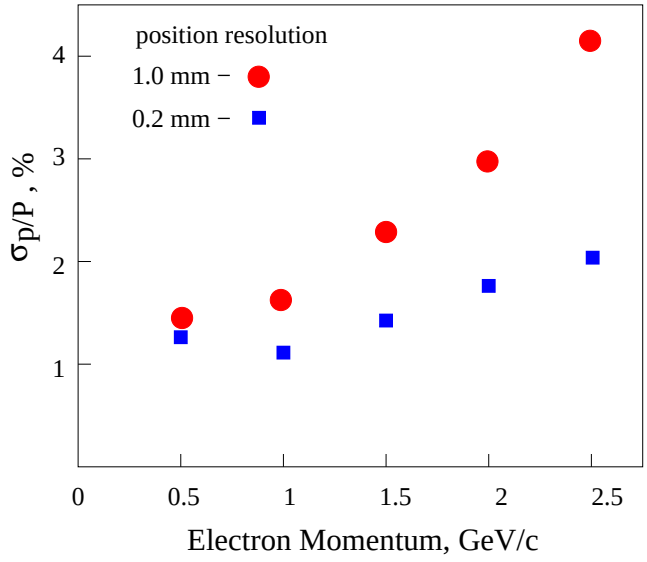

Figure 13: BigBite momentum resolution as function of the electron momentum assuming a position resolution from the MWDCs of 0.2 mm (blue squares), and 1.0 mm (red circles). These are the results of a complete Monte Carlo study of the BigBite spectrometer at 54° using a gaseous helium target.

Additional MC studies were done to evaluate the parameters of the proposed experiment. Figures 14 and 15 show line drawings of BigBite and the other experimental components as they were defined in the simulations.

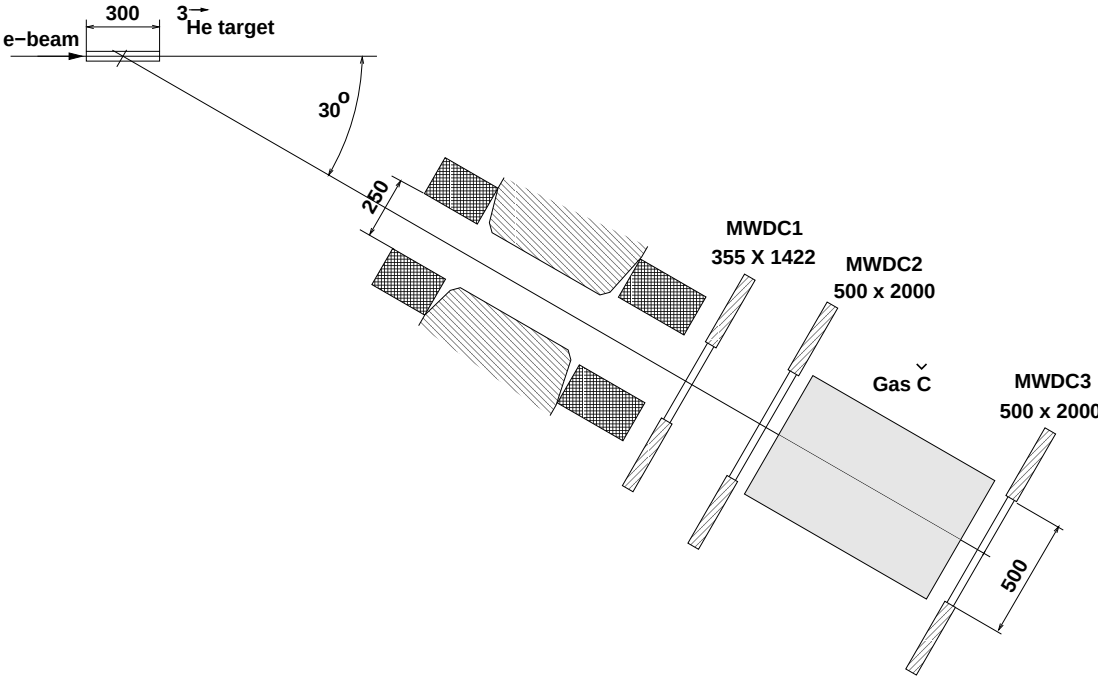

Figure 14: The top view of the experimental setup in the MC simulation. Dimensions are given in mm.

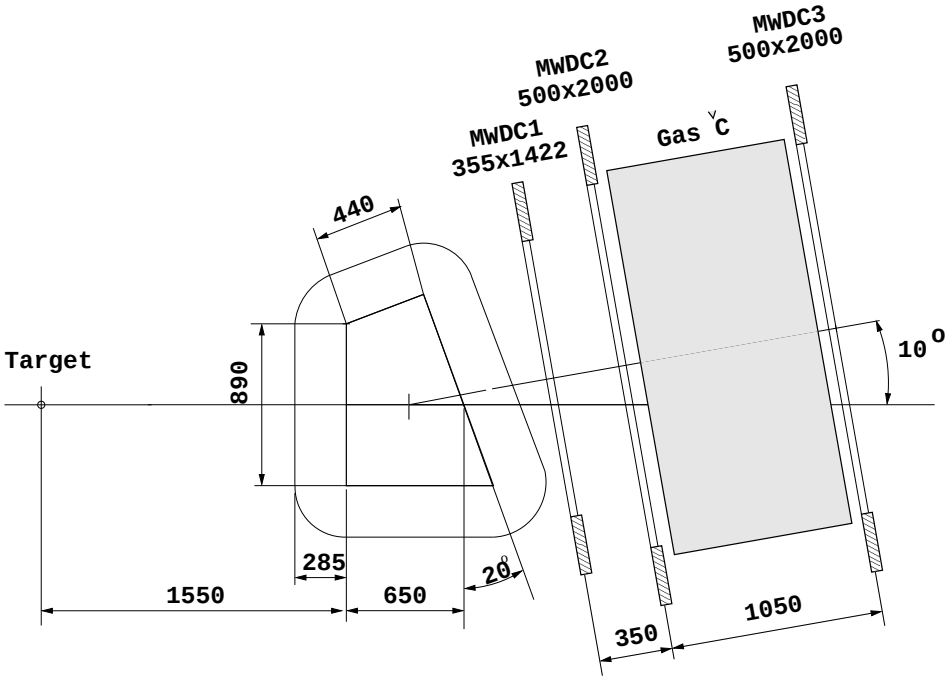

Figure 15: Side views of the experimental setup in the MC simulation. Dimensions are given in mm.

The BigBite solid angle acceptance for different positions along the target is shown in Fig. 16, where events were selected which had an electron momentum of 3.2 GeV/c and scattering angles of $30 \pm 4^{\circ}$. The target length can be represented as 30 cm/sin(θ). The solid angle averaged over the 30 cm target length is 50 msr.

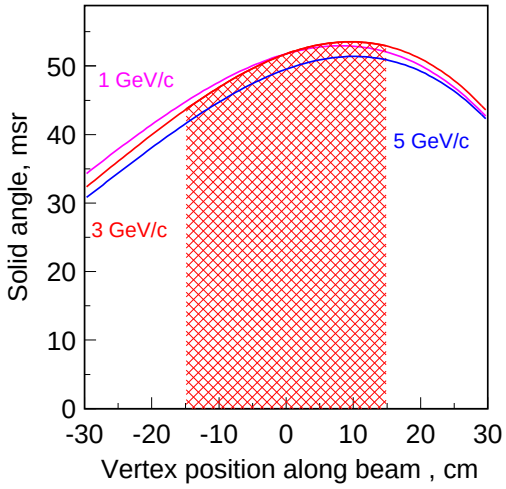

Figure 16: The MC simulation of the BigBite solid angle *vs.* the position on target along the beam direction.

5.4.3 The Field Clamp Configuration for BigBite

The operation of the polarized ^{3}He target requires small magnetic field gradients (the gradient averaged over the target volume must be below 30 mGauss/cm). When the BigBite spectrometer was used at NIKHEF with an internal ^{3}He target, it was found that the a field clamp covering only the coils (see Fig. 12) was sufficient to keep the gradient below 30 mGauss/cm for dipole excitations up to 0.9 Tesla. Above this level the fringe field of the saturated iron yoke created larger gradients. This proposal has BigBite running at a higher field (1.2 T), but also has the magnet positioned further from the target region (1.55 m *vs.* 1.1 m) so we anticipate the field gradient at the target would be comparable even if the old field clamp was used. Nevertheless, work is underway to design an improved clamp that will limit the field gradient to below 20 mGauss/cm in the target region.

5.4.4 BigBite Detector Package

For the proposed measurement, the BigBite detector package will consist of

- three Multi-wire Drift Chambers (MWDC) for tracking information,
- a gas Cerenkov counter between MWDC #1 and #2 for pion rejection,
- a double layer lead glass calorimeter for triggering on high energy electrons and for pion rejection, and
- a plane of scintillators.

The detector package configuration for BigBite similar to that of the G_{E_n} experiment with the addition of the gas Cerenkov counter that is being constructed for the Hall A neutron d_2 experiment (E06-014). Since the proposed experiment is inclusive, the addition of the Cerenkov counter for pion and proton rejection is critical.

The MWDC package was constructed at the University of Virginia. The package consists of three large MWDC, each with three groups of wire-planes with wires oriented at +60° (u), -60° (v), and +90° (x). Each group consists of two wire planes. The third group of wires (x) allows unambiguous track reconstruction in a high rate environment. Furthermore, the middle chamber allows the identification of multiple tracks at high rates. The active area of the first chamber is 35 cm $\times$ 140 cm while the active area of the second and third chambers is 50 cm $\times$ 200 cm. During the G_{E_n} experiment these MWDCs performed very well in a high rate environment where the rate of raw hits on each wire-plane was as high as 20 MHz. All 2600 wires in the chamber were operational for almost continuous running during the 2.5 month long experiment with no noisy or dead wires. The chamber resolution obtained during online analysis was approximately 300 μm, this is expected to improve to about 200 μm after further analysis. Figures 17 and 18 show the vertex reconstruction and momentum resolution achieved after online analysis of the G_{E_n} data.

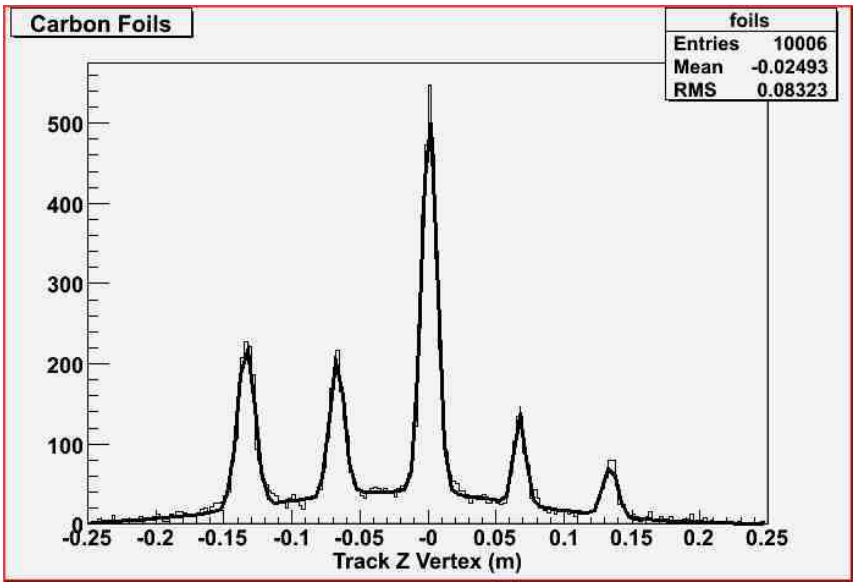

Figure 17: The vertex reconstruction of the ^{12}C foil target from online analysis of G_{E_n} data.

The electron identification for this proposal will be provided by the Cerenkov counter in combination with the electromagnetic calorimeter. The latter is composed by of two sub-packages. The first a preshower detector made out of blocks of TF-5 lead glass spanning an active area of $210 \times 74\,\mathrm{cm}^2$ with 10 cm depth (3 r.l.) along the particle direction. This is followed by a shower detector composed with total absorption blocks of TF-2 lead glass covering an area of $221 \times 85\,\mathrm{cm}^2$ with 34 cm depth which should contain showers with energies up to 10 GeV. The resolution of the calorimeter is about $8\%/\sqrt{(E)}$ leading to an expected pion rejection of 100:1.

The Cerenkov counter we plan to use for this experiment is currently being designed for the Hall A neutron d_2 experiment at 6 GeV (E06-014). It will be located in the gap between the first and second wire chambers with dimensions of 200x60x60 cm^3. Cerenkov radiation emitted by relativistic particles will be collected in 10 mirrors tiled in a 5x2 arrangement at the back of the chamber. Each of those primary mirrors focuses light into a 5" PMT by way of a flat secondary mirror located towards the front of the chamber. This configuration allows the PMTs to be positioned away from the BigBite fringe field and provides a relatively

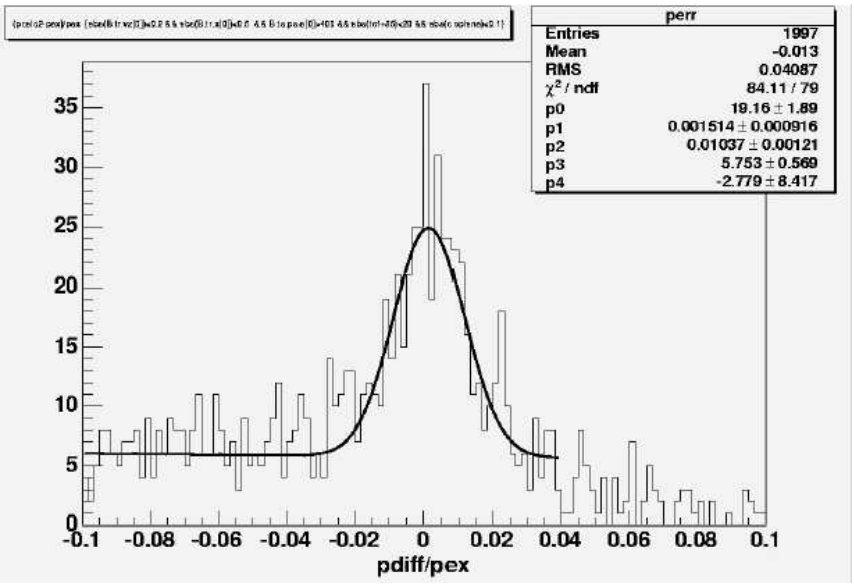

Figure 18: Reconstructed momentum *vs.* scattering angle showing the momentum resolution for the H(e,e') elastic data from G_{E_n} online analysis.

compact design that can be installed in the existing BigBite detector frame with minimal modifications.

Our preferred choice of Cerenkov radiator is C_4F_{10} at 1 atm. This material is non-flammable, non-toxic, odorless, and does not require special handling to remain a gas at room temperature. It is currently in use in Cherenkov devices in both Hall B and Hall C at Jefferson Lab. Its index of refraction is 1.0015 giving a pion threshold of 2.5 GeV/c. Assuming a 40 cm track length in the radiator, our calculations predicts a mean PMT response of 13 measured photo-electrons (p.e.'s) per electron with a conventional Burle 8854 5" PMT. This estimate includes the PMT quantum efficiency, PMT window transparency, and is multiplied by a factor of 0.7 to accommodate a cumulative 10% loss at each mirror and the PMT surface (the latter may be conservative). As a cross-check on the above calculation, the performance of the current Hall A short Cerenkov (a similar design) was scaled to correct for the different path-length and radiator gas. The resulting estimate of 12 p.e.'s for the BigBite Cerenkov configuration is consistent with the earlier calculation.

The high number of registered p.e.'s allow a aggressive online threshold (3–4 p.e.'s) to be applied which essentially removes all of the 1–2 p.e. background noise while triggering on $>98\%$ of the electron tracks (with a healthy margin of error).

We expect a pion rejection ratio of at least 1000:1 and, when coupled with cuts on the shower/pre-shower, we expect to achieve a total pion rejection of 10^5. This is more than adequate for the proposed measurement. The pion asymmetry will also be measured during the same experiment.

We also reserve the option of adding wavelength shifter to the PMT surface to convert some fraction of the far-UV photons to something in the PMT sensitivity envelope. This typically results in a 20-30% increase in the number of p.e.'s registered by the PMT, although getting the coating 'just right' is a bit of an art. This would allow us to switch to an alternate radiator gas such as Freon12 ($n = 1.0011, p_\pi^{\text{thresh}} = 3\,\text{GeV}$) with a negligible impact on the Cerenkov performance.

5.4.5 Left High Resolution Spectrometer

The Hall A left High Resolution Spectrometer (HRS) will be positioned on the opposite side of the beamline at the same angle as BigBite. This will allow it to measure absolute cross sections in the same x range as the

the BigBite spectrometer. We will use the left HRS with its standard detector package for electrons which consists of:

- two vertical Drift Chambers (VDCs) for the measurement of momentum and production angle,
- a Threshold Gas Cherenkov counter for pion rejection,
- a set of scintillators for triggering on charged particles, and
- a double layer lead glass calorimeter for additional pion rejection.

As the E99-117 analysis shows, the pion rejection factor with the Cherenkov counter and the lead glass calorimeter are better than 1×10^5 with an electron detection efficiency of 98%. This is sufficient for our worst case scenario.

Specific advantages make the HRS spectrometer a well matched tool for the proposed measurement.

- Good electron events in the spectrometer are, in principle, due only to electron scattering off ^{3}He nuclei since the target cell glass windows are outside the spectrometer acceptance. However, excellent target reconstruction by the HRS spectrometers allows for even better background rejection.
- The excellent resolution of the spectrometer permits the measurement of elastic scattering off ^{3}He needed for an absolute calibration of the detector in order to measure absolute cross sections.

6 Corrections and systematic uncertainties for g_2^n and d_2^n

6.1 Radiative Corrections

The radiative corrections (RC) will be performed in two stages. First, the internal corrections will be evaluated following the procedure developed by Bardin and Shumeiko[45] for the unpolarized case and extended to the spin dependent lepto-production cross sections by Akushevish and Shumeiko[57, 58]. Second, using these internally corrected cross sections, the external corrections (for thick targets) are applied by extending the procedure developed for the unpolarized cross sections by Tsai[59, 60] with modifications appropriate for this experiment.

The present measurement is self sufficient to provide input data for the iterative unfolding procedure used in the radiative corrections of these same data, except for the lowest momentum transfer region. However previous measurements at JLab at 6 GeV provide for the remaining input data to complete this process with no need for input models. This is important since we are interested in providing for helicity dependent cross sections not only in the deep inelastic region where world fits of structure functions are available but also the resonance region where modeling is still tentative especially for a nucleus like ^{3}He.

6.2 Spin Structure Functions: From ^{3}He to the Neutron

Because the deuteron polarization is shared roughly equally between the proton and neutron, extraction of neutron spin structure functions requires a precise knowledge of the proton spin structure, in addition to the nuclear effects [62]. This problem is compounded by the fact that the spin-dependent structure functions of the proton are typically much larger than those of the neutron, making extraction of the latter especially sensitive to small uncertainties in the proton structure functions. In ^{3}He, however, the neutron carries almost 90% of the nuclear spin making polarized ^{3}He an ideal source of polarized neutrons.

The three-nucleon system has been studied for many years, and modern three-body wave functions have been tested against a large array of observables which put rather strong constraints on the nuclear models [63]. In particular, over the past decade considerable experience has been acquired in the application of three-body wave functions to deep-inelastic scattering [64, 65, 66].

The conventional approach employed in calculating nuclear structure functions in the region $0.3 < x < 0.8$ is the impulse approximation, in which the virtual photon scatters incoherently from individual nucleons in the nucleus [67]. Corrections due to multiple scattering, NN correlations or multi-quark effects are usually confined to either the small-x ($x < 0.2$), or very large-x ($x > 0.9$) regions. In the impulse approximation the g_1 structure function of ^{3}He, in the Björken limit ($Q^2, \nu \to \infty$), is obtained by folding the nucleon structure function with the nucleon momentum distribution Δf_N ($N = p, n$) in ^{3}He:

$$g_1^{^3\mathrm{He}}(x) \;=\; \int_x^3 \frac{dy}{y}\,\left\{2\Delta f_p(y)\; g_1^p(x/y) \;+\Delta f_n(y)\; g_1^n(x/y)\right\}, \tag{22}$$

where y is the fraction of the ^{3}He momentum carried by the nucleon, and the dependence on the scale, Q^2, has been suppressed. The nucleon momentum distributions $\Delta f_N(y)$ are calculated from the three-body nuclear wave function, which are obtained by either solving the Faddeev equation [68] or using variational methods [65], and are normalized such that:

$$\int_0^3 dy\,\Delta f_N(y) \;=\; \rho_N\,, \tag{23}$$

where ρ_N is the polarization of the nucleon in ^{3}He. While the full three-body wave function involves summing over many channels, in practice the three lowest states, namely the S, S' and D, account for over 99% of the normalization. Typically, one finds $\rho_n \approx 87\%$ and $\rho_p \approx -2\%$ [63, 64, 65, 66, 68].

The smearing in Eqn.(22) incorporates the effects of Fermi motion and nuclear binding. Correctly accounting for these effects is important when attempting to extract information on nucleon structure functions from nuclear data at $x > 0.6$, as well as for determining higher moments of structure functions, in which the large-x region is more strongly weighted.

The nuclear corrections to the g_2^n structure function can be evaluated analogously to those for g_1^n. One can estimate the order of magnitude of the effects by considering firstly the twist-2 part of g_2^n, which is determined from g_1^n through the Wandzura-Wilczek relation [42, 70]:

$$g_2^{^3\mathrm{He}}(x)\Big|_{\mathrm{tw-2}} \;=\; -g_1^{^3\mathrm{He}}(x) \;+\; \int_x^3 \frac{dy}{y}\, g_1^{^3\mathrm{He}}(x/y)\;, \tag{24}$$

where $g_1^{^3\mathrm{He}}$ is given by Eqn.(22). The main effect numerically at moderate to large x is due to the difference between the neutron and ^{3}He polarizations, as the effects due to smearing peaks at the level of a few percent at $x \sim 0.6$. Similarly, the difference in the second moments of $g_2^{^3\mathrm{He}}$ between the convolution results using different ^{3}He wave functions is a few percent [68,69]. Moreover, since the main objective of the experiment is to extract the second moment of $3g_2^n + 2g_1^n$, namely $\int dx\, x^2(3g_2^n(x) + 2g_1^n(x))$, the sensitivity of the correction to x variations of the integrand is reduced compared to a direct extraction of the g_2 or g_1 structure functions themselves. degli Atti [65] showed that nuclear binding effects are quite sizable for g_1^n in the resonance region at Q^2 values of $1\,\mathrm{GeV}^2/c^2$ when extracted from polarized ^{3}He. However, the nuclear effects are small $< 4\%$ in the DIS region ($Q^2 = 10\,\mathrm{GeV}^2/c^2$). Our own data, taken during the Bloom-Gilman duality experiment (E01-012), show that the resonance structures disappear for Q^2 $/gtrsim\, 3\,\mathrm{GeV}^2/c^2$.

While the nuclear model dependence of the nuclear correction appears to be relatively weak for the twist-2 approximation in the Björken limit, an important question for the kinematics relevant to this experiment is how are these effects likely to be modified at finite Q^2? To address this question one needs to obtain generalizations of Eqns. (22) and (24) which are valid at any Q^2, and which can incorporate the twist-3 component of g_2. In fact, at finite Q^2 one finds contributions from g_1^N to $g_2^{^3\mathrm{He}}$, and from g_2^N to $g_1^{^3\mathrm{He}}$. The latter vanish in the Björken limit, but the former are finite, although they depend on the Fermi momentum of the bound nucleons. These corrections can be calculated by working directly in terms of the (unintegrated) spectral function $S(\vec{p},E)$, where p is the bound nucleon momentum and E is the separation energy, rather than in terms of the momentum distribution functions $\Delta f_N(y)$. Following Schulze & Sauer [66], it is convenient to parametrize the ^{3}He spectral function according to:

$$S(\vec{p},E) \;=\; \frac{1}{2}\left(f_0 + f_1 \vec{\sigma}_N\cdot\vec{\sigma}_A + f_2\left[\vec{\sigma}_N\cdot\hat{p}\;\vec{\sigma}_A\cdot\hat{p} \;-\frac{1}{3}\vec{\sigma}_N\cdot\vec{\sigma}_A\right]\right)\;, \tag{25}$$

where $\vec{\sigma}_N$ and $\vec{\sigma}_A$ are the spin operators of the nucleon and ^{3}He, respectively, and the functions $f_{0,1,2}$ are scalar functions of $|\vec{p}|$ and E. The function f_0 contributes to unpolarized scattering only, while f_1 and f_2 determine the spin-dependent structure functions. In terms of these functions, at finite Q^2 one has a set of

coupled equations for $g_1^{^3\mathrm{He}}$ and $g_2^{^3\mathrm{He}}$ [72]:

$$
\begin{aligned}
& x g_1^{^3\mathrm{He}}(x,Q^2) + (1-\gamma^2) x g_2^{^3\mathrm{He}}(x,Q^2) \\
= & \sum_{N=p,n} \int d^3p\, dE\, (1-\frac{\varepsilon}{M}) \left\{ \left[\left(1 + \frac{\gamma p_z}{M} + \frac{p_z^2}{M^2} \right) f_1 + \left(-\frac{1}{3} + \hat{p}_z^2 + \frac{2\gamma p_z}{3M} + \frac{2p_z^2}{3M^2} \right) f_2 \right] z g_1^N(z,Q^2) \right. \\
& \left. + (1-\gamma^2)(1 + \frac{\varepsilon}{M} \left[f_1 + \left(\frac{p_z^2}{\vec{p}^2} - \frac{1}{3} \right) f_2 \right] \frac{z^2}{x} g_2^N(z,Q^2) \right\} , \qquad (26)
\end{aligned}
$$

$$
\begin{aligned}
& x g_1^{^3\mathrm{He}}(x,Q^2) + x g_2^{^3\mathrm{He}}(x,Q^2) \\
= & \sum_{N=p,n} \int d^3p\, dE\, (1-\frac{\varepsilon}{M}) \left\{ \left[\left(1 + \frac{p_x^2}{M^2} \right) f_1 + \left(\vec{p}_x^2 - \frac{1}{3} + \frac{2p_x^2}{3M^2} \right) f_2 \right] z g_1^N(z,Q^2) \right. \\
& \left. + \left[\left(1 + \frac{p_x^2}{M^2}(1-z/x) \right) f_1 + \left(\vec{p}_x^2 - \frac{1}{3} + \frac{2p_x^2}{3M^2}(1-z/x) - \frac{\gamma p_z \hat{p}_x^2}{M} \frac{z}{x} \right) f_2 \right] z g_2^N(z,Q^2) \right\} , \qquad (27)
\end{aligned}
$$

with $\gamma = \sqrt{1+4M^2x^2/Q^2}$ a kinematic factor parametrizing the finite Q^2 correction, $\varepsilon \equiv \vec{p}^2/4M - E$, and $z = x/(1+(\varepsilon+\gamma p_z)/M)$. Equations (26) and (27) can then be solved to obtain $g_1^{^3\mathrm{He}}$ and $g_2^{^3\mathrm{He}}$ explicitly. For $Q^2 \to \infty$ Eqns. (26) and (27) reduce to simple one-dimensional convolution expressions, as in Eqn. (22). At finite Q^2, however, the smearing function effectively becomes x and Q^2 dependent, so that the amount of smearing in general will depend on the shape of the nucleon structure functions.

The nuclear correction of most interest for this experiment is that to the g_2 structure function. One can test the sensitivity to the kinematic Q^2 dependence, as distinct from the Q^2 dependence in the nucleon structure function itself, by taking the same input neutron structure function for all values of Q^2 at which $x g_2^{^3\mathrm{He}}$ is evaluated. One finds [72] that the effect of the kinematic Q^2 dependence turns out to be rather small at $Q^2 \sim$ 1–4 GeV^2, and only becomes noticeable for low $Q^2 \sim 0.2$ GeV^2. Furthermore, at these values of Q^2 the g_1^n contribution to $g_2^{^3\mathrm{He}}$ is negligible compared with the lowest order neutron polarization correction. This confirms earlier analyses of the nuclear corrections by the Rome-Perugia group [73].

There was also an investigation in Ref. [71] into the role of the $\Delta(1232)$ in deep-inelastic scattering on polarized ^{3}He and its effects on the g_1 neutron spin structure function extraction. The authors estimated that when taking the effect of the Δ into account the values of the first moment of g_1^n increases by 6—8 %.

In summary, all of the nuclear structure function analyses that have been performed suggest that both the neutron g_1^n and g_2^n structure functions can be extracted from ^{3}He data with minimal uncertainties associated with nuclear corrections. Estimating all the corrections and their uncertainties we come to the conclusion that in this experiment the statistical error on the final result is still the dominant error.

6.3 Target Spin Misalignment

One item of concern was the effect of the target relative spin misalignment between the transverse and longitudinal direction measurements. Fig. 19 shows this effect at each value of x on the integrand of d_2. Calculations assuming a relative error of 0.5° in the relative direction of the transverse versus perpendicular results in a relative error $\Delta d_2/d_2 = 0.15\%$. Using the Weigel *et al.* [61] model of g_2 and g_1 we estimated $\Delta d_2/d_2$ to be of the order of 10 % and thus an absolute systematic uncertainty of about $1.5 \cdot 10^{-3}$. Recent implementation of a precision air compass (used during G_{E_n} in Hall A) have reduced the uncertainty in the target spin alignment measurement to better than 0.1° suggesting a more realistic (but still conservative) estimate would be $< 5 \times 10^{-4}$.

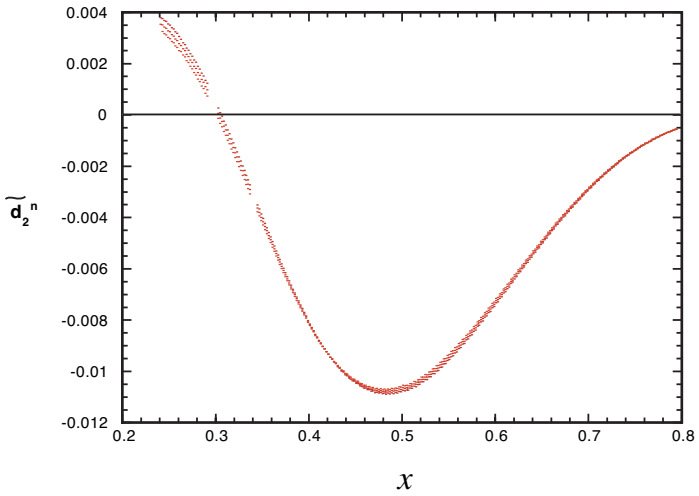

Figure 19: Effect of target relative spin misalignment by 0.5° between the transverse and longitudinal measurements

6.4 Summary of Systematic Uncertainties

To evaluate the remaining experimental systematic uncertainties for g_2^n and d_2^n we used relative uncertainties in the cross sections and asymmetries achieved in JLab E94-010, E97-103 and E99-117. Table 6.4 summarizes these estimates.

With our improved projected statistical precision the total uncertainty in the measured quantities will be almost equally shared between the statistical and the systematic accuracy of the measurement.

An elastic scattering asymmetry measurement is planned at low energy (E_i = 2.2 GeV) using the HRS spectrometer to calibrate our spin dependent absolute cross sections. This quantity can be evaluated using the measured electric and magnetic form factors of ^{3}He. This measurement would actually determine the polarization of the ^{3}He nuclei along the electron beam path. False asymmetries will be checked to be consistent with zero by comparing data with target spins in opposite directions.

Also contributing to the dilution of the asymmetry is the pair-electron contamination. This correction is x dependent, and is relevant only in the low x region. This contamination will be measured in this experiment by reversing the spectrometer polarity on the LHRS spectrometer.

Table 4: List of the systematic error contributions to g_2^n and d_2^n

Item description	Subitem description	Relative uncertainty
Target polarization		1.5 %
Beam polarization		3 %
Asymmetry (raw)		
	• Target spin direction (0.1°)	$< 5 \times 10^{-4}$
	• Beam charge asymmetry	< 50 ppm
Cross section (raw)		
	• PID efficiency	< 1 %
	• Background Rejection efficiency	≈ 1 %
	• Beam charge	$<$ 1 %
	• Beam position	$<$ 1 %
	• Acceptance cut	2-3 %
	• Target density	< 2%
	• Nitrogen dilution	< 1%
	• Dead time	<1%
	• Finite Acceptance cut	<1%
Radiative corrections		≤ 5 %
From ^{3}He to Neutron correction		5 %
Total systematic uncertainty (for both $g_2^n(x,Q^2)$ and $d_2(Q^2)$)		≤ 10 %
Estimate of contributions to d_2 from unmeasured region	$\int_{0.003}^{0.23} \tilde{d}_2^n \, dx$	4.8×10^{-4}
Projected absolute statistical uncertainty on d_2		$\Delta d_2 \approx 5 \times 10^{-4}$
Projected absolute systematic uncertainty on d_2 (*assuming* $d_2 = 5 \times 10^{-3}$)		$\Delta d_2 \approx 5 \times 10^{-4}$

7 Summary

7.1 The Proposal in Hall A

In summary, we request 700 hours (29 days) of beam to measure the unpolarized cross section $\sigma_0^{^3He}$, the parallel asymmetry $A_\parallel^{^3He}$ and the perpendicular asymmetry $A_\perp^{^3He}$. The request involves 200 hours for the 6.6 GeV kinematics, 400 hours for the 8.8 GeV settings, and an additional 100 hours for calibration and overhead.

Those data will be used to extract the g_2^n structure function on the neutron in the large-x, large-Q^2 region with good precision (Figures 20 and 21). In marked contrast to g_1^n, the Q^2 evolution of g_2^n is largely a mystery for $Q^2 > 1\mathrm{GeV}^2/c^2$. The large Q^2 coverage of the proposed experiment will allow a clean measurement of the Q^2 behavior $g_2^n(x,Q^2)$ for $x > 0.5$ for the very first time. Figure 22 is a plot of the kinematic coverage for this proposal.

The data from this measurement will also be combined with those of the lower energy d_2^n measurement E04-016 to evaluate d_2^n for $< Q^2 >= \mathrm{GeV}^2/c^2$. This will provide a measure of the Q^2 dependence of the d_2^n matrix element, again for the very first time for $Q^2 > 1\,\mathrm{GeV}^2/c^2$. The quantity $d_2^n = \int_0^1 \bar{g}_2\, dx = \int_0^1 x^2(2g_1 + 3g_2)\, dx$ is related to the twist three matrix element in the Operator Product Expansion (OPE) framework. It is a direct measure of the quark-gluon correlations within the nucleon and reflects the response of the *color* electric and magnetic fields to the polarization of the nucleon (alignment of its spin along one direction). This quantity has seen considerable study in Lattice QCD and is one of the cleanest observables with which to test the theory.

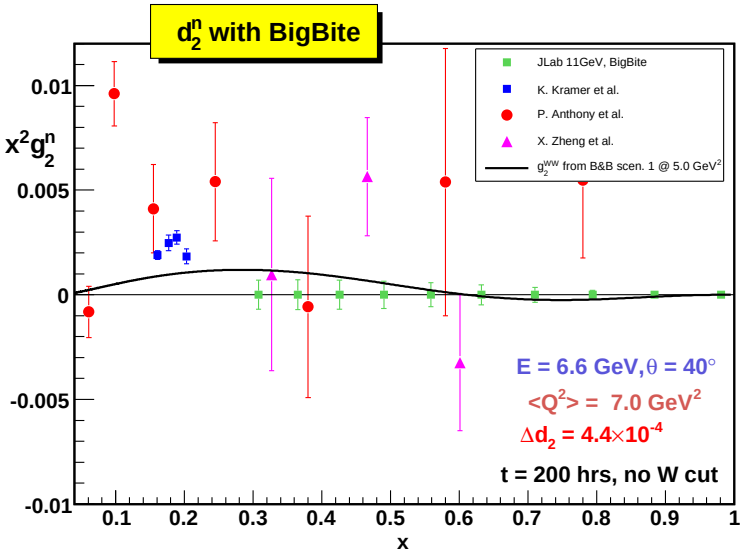

Figure 20: $x^2 g_2^n(x)$ *vs.* x presenting the statistical errors expected from the proposed measurement (green squares) for the 6.6 GeV kinematics. Existing world data are also shown. Note that these points reflect a wide range of Q^2 values. d_2 will be evaluated by combining the data at both kinematics and evolving integrand to a common Q^2, bounding the uncertainty introduced by the evolution of g_2 by exploiting the explicitly measured Q^2 evolution.

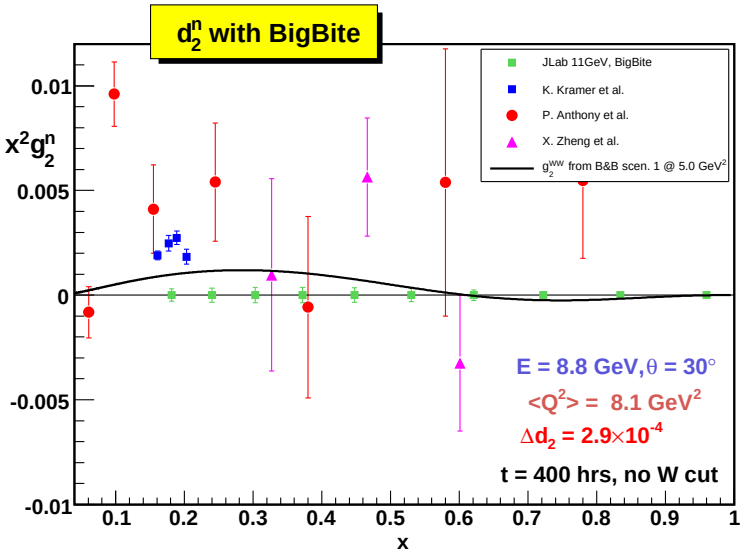

Figure 21: $x^2 g_2^n(x)$ *vs.* x presenting the statistical errors expected from the proposed measurement (green squares) for the 6.6 GeV kinematics. Existing world data are also shown. As in Figure 20, these points reflect a wide range of Q^2 values. d_2 will be evaluated by combining the data at both kinematics and evolving the integrand to a common Q^2.

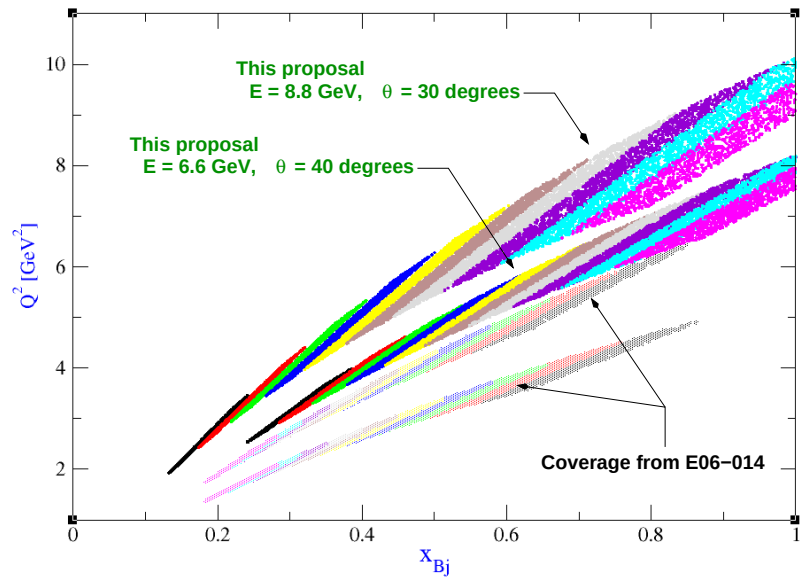

Figure 22: The two upper stripes reflect the BigBite (x, Q^2) coverage for the proposed measurement at 6.6 and 8.8 GeV. The colored subdivisions within each kinematic stripe reflect how the BigBite data will be divided into bins offline. The HRS kinematics are chosen to match the central (x, Q^2) value for each of those bins. The lower stripes reflect the coverage from the lower energy measurement E06-014.

7.2 The *Complementary* Proposal in Hall C

We would also like to comment on a "sister" proposal for Hall C (also requesting 700 hours) that has also been submitted to the PAC30 board. The kinematic coverage of the Hall A measurement has been specifically selected to compliment the coverage of the Hall C proposal. BigBite in Hall A is ideally suited to map out the the high-x, high-Q^2 region with excellent statistics in a modest time. In contrast, the SHMS/HMS in Hall C is uniquely suited to make a *definitive* measurement of the Q^2 evolution of d_2^n in the central Q^2 range due to its uniquely flat Q^2 coverage per bin over $0.4 < x < 1$. This allows d_2 to be explicitly evaluated at several Q^2 values *without* evolving the integrand. An open geometry detector like BigBite is not able to match such kinematics due to rate limitations at forward angles. Figure 23 shows the combined coverage of the pair of proposed measurement in Halls A and C and highlights proposed lines of integration for d_2 and regions of study for the Q^2 evolution of g_2. The information that could be extracted from such a combined effort is truly impressive.

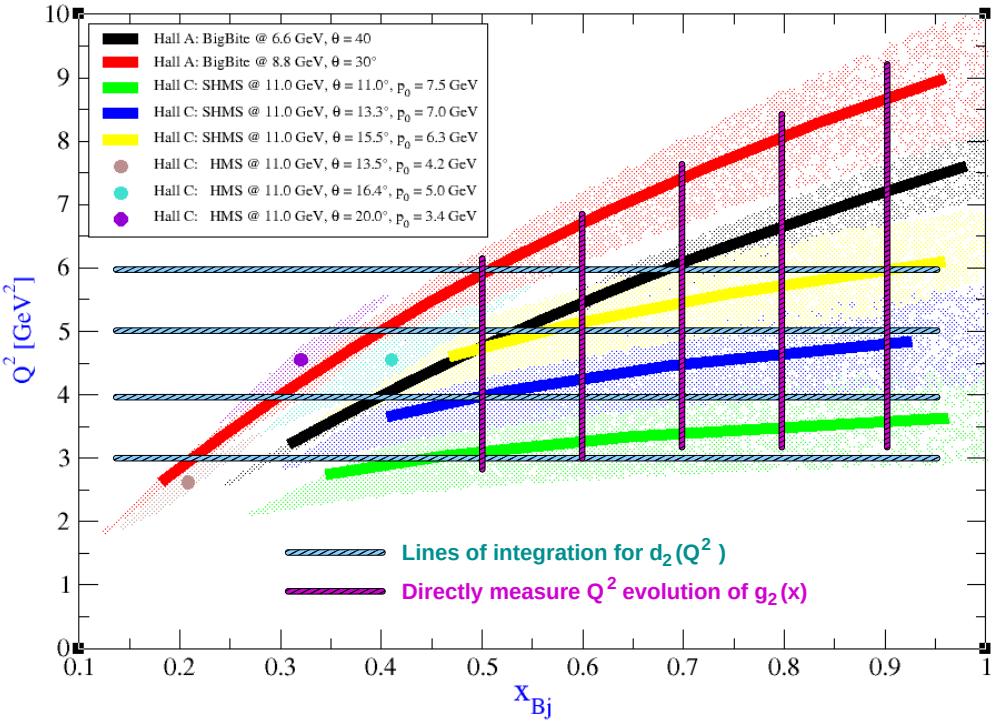

Figure 23: The combined kinematic coverage for the pair of complimentary experiments proposed in Halls A and C. In addition to simply mapping out $g_2(x, Q^2)$ over a very broad range of x and Q^2, the vertical lines show the x values where a thorough Q^2 evolution study can be accomplished. The horizontal lines show how the combined data could be binned to compute $d_2^n(Q^2)$ at almost constant Q^2 for a broad range of Q^2.

8 Bibliography

References

[1] A.D. Martin, R.G. Roberts, W.J. Stirling, R.S. Thorne; hep-ph/0201127.

[2] J. Pumplin et al.; hep-ph/0303013.

[3] H1 Collaboration; C. Adloff et al., Eur. Phys. J. C30, 1 (2003).

[4] P. Bosted, CLAS-NOTE-2004-005.

[5] D.E. Wiser, Ph.D. thesis, Univ. of Wisconsin, 1977.

[6] E. Shuryak and A. Vainshtein, Nuc. Phys. B **201** (1982) 141.

[7] R. L. Jaffe and X. Ji, Phys. Rev. D **43** (1991) 724.

[8] B. W. Filippone and X. Ji, Adv. in Nucl. Phys. **26**, 1 (2001).

[9] S. Wandzura and F. Wilczek, Phys. Lett. B **72**, 195 (1977).

[10] E. Stein, P. Gornicki, L. Mankiewicz and A. Schäfer, Phys. Lett. B 353, 107 (1995).

[11] X. Ji, arXiv:hep-ph/9510362.

[12] X. Ji and P. Unrau, Phys. Lett. B **333** (1994) 228.

[13] X. Ji Nucl. Phys. **B402** (1993) 217.

[14] S. A. Larin, T. van Ritbergen and J.A. Vermaseren, Phys. Lett. **404**, 153 (1997); S. A. Larin, Phys. Lett. B **334**, 192 (1994).

[15] F. E. Close and R. G. Roberts, Phys. Lett. B **336**, 257 (1994).

[16] X. Ji and W. Melnitchouk, Phys. Rev. D **56**, 1 (1997).

[17] J. Edelmann, G. Piller, W. Weise, N. Kaiser, Nucl. Phys. A **665** (2000) 125.

[18] S. Simula, M. Osipenko, G. Ricco and M. Tauiti, hep/0205118 and references therein.

[19] M. Osipenko *et al.*, Phys. Lett. B **609**, 259 (2005) [arXiv:hep-ph/0404195].

[20] Z. E. Meziani *et al.*, Phys. Lett. B **613**, 148 (2005) [arXiv:hep-ph/0404066].

[21] A. Deur *et al.*, Phys. Rev. Lett. **93**, 212001 (2004) [arXiv:hep-ex/0407007].

[22] A. V. Sidorov and C. Weiss, Phys. Rev. D **73**, 074016 (2006) [arXiv:hep-ph/0602142].

[23] X. Ji, in Proceeding of the Workshop on Deep Inelastic scattering and QCD, Editors: JF. Laporte et Y. Sirois Paris, France, 24-28 April, 1995 (ISBN 2-7302-0341-4).

[24] P. L. Anthony *et al.* [E155 Collaboration], Phys. Lett. B **458**, 529 (1999) [arXiv:hep-ex/9901006].

[25] H. Burkhardt and W. N. Cottingham, Ann. Phys. **56** (1970) 453.

[26] R. Jaffe, Comments Nucl. Part. Phys. 19 (1990) 239.

[27] I. P. Ivanov *et al.*, Phys. Rep. **320**, 175 (1999).

[28] M. Anselmino, A. Efremov and E. Leader, Phys. Rep. **261**, 1 (1995).

[29] G. Altarelli, B. Lampe, P. Nason and G. Ridolfi, Phys. Lett. B **334**, 187 (1994).

[30] M. Amarian *et al.*, Phys. Rev. Lett. **89**, 242301 (2002).

[31] M. Amarian *et al.*, Phys. Rev. Lett. **92**, 022301 (2004).

[32] D. Adams *et al.*, Phys. Lett. **B336** (1994) 125.

[33] P. L. Anthony *et al.*, Phys. Rev. Lett. **71** (1993) 959.

[34] P. L. Anthony *et al.*, Phys. Rev. D **54** (1996) 6620.

[35] K. Abe *et al.*, Phys. Rev. Lett. **76** (1996) 587.

[36] K. Abe *et al.*, Phys. Lett. B **404** (1997) 377.

[37] P. L. Anthony *et al.*, Phys. Lett. B**458** (1999) 529.

[38] P. L. Anthony *et al.* [E155x Collaboration], Phys. Lett. B **553**, 18 (2003) [arXiv:hep-ex/0204028].

[39] X. Zheng *et al.* [Jefferson Lab Hall A Collaboration], Phys. Rev. C **70**, 065207 (2004) [arXiv:nucl-ex/0405006].

[40] K. Kramer *et al.*, Phys. Rev. Lett. **95**, 142002 (2005) [arXiv:nucl-ex/0506005].

[41] K. Abe *et al.*, Phys. Rev. D **58** (1998) 112003-1.

[42] S. Wandzura and F. Wilczek, Phys. Lett. B **72** (1977) 195.

[43] JLab E01-012 experiment, Spokespeople N. Liyanage, J. P. Chen and Seonho Choi.

[44] JLab E01-006 experiment, Spokesperson O. Rondon and M. Jones

[45] D. Yu. Bardin and N. M. Shumeiko, Nucl. Phys. B **127** (1977) 1251.

[46] M. Wakamatsu, Phys. Lett B **487** (2000) 118.

[47] M. Stratmann, Z. Phys. C **60** (1993) 763.

[48] E. Stein, Phys. Lett. B **343** (1995) 369.

[49] B. Ehrnsperger, A Schäfer, Phys. Rev. D **52** (1995) 2709.

[50] I. Balitsky, V. Barun, A. Kolesnichenko, Phys. Lett. B **242** (1990) 245; B **318** (1995) 648 (E).

[51] M. Gockeler *et al.*, Phys. Rev. D **72**, 054507 (2005) [arXiv:hep-lat/0506017].

[52] M. Gockeler *et al.*, Phys. Rev. D **63**, 074506 (2001), [hep-lat/0011091].

[53] R. G. Edwards *et al.* [LHPC Collaboration], Private communication

[54] C. R. V. Bourrely, J. Soffer and F. Buccella, Eur. Phys. J. C **41**, 327 (2005) [arXiv:hep-ph/0502180].

[55] D. Drechsel, S. Kamalov and L. Tiator, Phys. Rev. D **63**, 114010 (2001).

[56] C. W. Kao, T. Spitzenberg and M. Vanderhaeghen, Phys. Rev. D **67**, 016001 (2003).

[57] T.V. Kuchto and N. M. Shumeiko, Nucl. Phys. B **219** (1983) 412.

[58] I. V. Akushevich and N. M. Shumeiko, J. Phys. **G**: Nucl. Part. Phys. **20** (1994) 513.

[59] L. W. Mo and Y. S. Tsai, Rev. Mod. Phys. **41** (1969) 205.

[60] Y. S. Tsai, SLAC-PUB-848 (1971).

[61] H. Weigel, L. Gamberg, H. Reinhart, Phys. Rev. D**55** (1997) 6910.

[62] W. Melnitchouk, G. Piller and A.W. Thomas, Phys. Lett. B **346** (1995) 165; S. A Kulagin, W. Melnitchouk, G. Piller and W. Weise Phys. Rev. C **52** (1995) 932.

[63] J.L. Friar et al., Phys. Rev. C **42** (1990) 2310.

[64] R.M. Woloshyn, Nucl. Phys. A **496** (1989) 749.

[65] C. Ciofi degli Atti, E. Pace and G. Salme, Phys. Rev. C **46** (1992) R1591; C. Ciofi degli Atti, S. Scopetta, E. Pace, G. Salme, Phys. Rev. C **48** (1993) 968;

[66] R.W. Schulze and P.U. Sauer, Phys. Rev. C **48** (1993) 38.

[67] D.F. Geesaman, K. Saito and A.W. Thomas, Ann. Rev. Nucl. Part. Sci. **45** (1995) 337.

[68] I.R. Afnan, F. Bissey and A.W. Thomas, Phys. Rev. C**64** (2001) 024004.

[69] I.R. Afnan, F. Bissey, J. Gomez, A.T. Katramatou, W. Melnitchouk, G.G. Petratos and A.W. Thomas, Phys. Lett. B **493** (2000) 36.

[70] F. Bissey, W. Melnitchouk, A. W. Thomas, in preparation.

[71] C. Boros, V. Guzey, M. Strikman, A.W. Thomas, Phys. Rev. **D64** (2001) 014025 and hep-ph/0008064.

[72] S.A. Kulagin and W. Melnitchouk, in preparation.

[73] S. Scopetta, private communication.

[74] J. Alcorn *et al.*, Nucl. Inst. Meth. A **522** (2004) 294.

[75] G. Cates *et al.*, Jefferson Lab E02-013 Proposal, http://www.jlab.org/exp_prog/proposals/02/PR02-013.pdf.

[76] E. Babcock *et al.*, Phys. Rev. Lett. **91** (2003) 123003.

[77] D. J. J. de Lange *et al.*, Nucl. Instr. and Meth. **A 406**, 182 (1998).

[78] D. J. J. de Lange *et al.*, Nucl. Instr. and Meth. **A 412**, 254 (1998).

[79] V. Nelyubin, private communication.

[80] S. Nanda and D. Lhuillier, Conceptual Design for Hall A Compton Polarimetry Upgrade http://www.jlab.org/∼nanda/compton/doc/compton_upgrade.pdf